NEUROSCIENCE

Human pluripotent stem cell–derived brain pericyte–like cells induce blood-brain barrier properties

Matthew J. Stebbins[1*†], Benjamin D. Gastfriend[1†], Scott G. Canfield[1‡], Ming-Song Lee[2], Drew Richards[1], Madeline G. Faubion[1§], Wan-Ju Li[2], Richard Daneman[3], Sean P. Palecek[1‖], Eric V. Shusta[1‖]

Brain pericytes play important roles in the formation and maintenance of the neurovascular unit (NVU), and their dysfunction has been implicated in central nervous system disorders. While human pluripotent stem cells (hPSCs) have been used to model other NVU cell types, including brain microvascular endothelial cells (BMECs), astrocytes, and neurons, hPSC-derived brain pericyte–like cells have not been integrated into these models. In this study, we generated neural crest stem cells (NCSCs), the embryonic precursor to forebrain pericytes, from hPSCs and subsequently differentiated NCSCs to brain pericyte–like cells. These cells closely resembled primary human brain pericytes and self-assembled with endothelial cells. The brain pericyte–like cells induced blood-brain barrier properties in BMECs, including barrier enhancement and reduced transcytosis. Last, brain pericyte–like cells were incorporated with iPSC-derived BMECs, astrocytes, and neurons to form an isogenic human model that should prove useful for the study of the NVU.

INTRODUCTION

The blood-brain barrier (BBB) is composed of specialized brain microvascular endothelial cells (BMECs) that line the vasculature of the central nervous system (CNS). BMECs allow for the selective passage of essential nutrients and metabolites into the brain and help prevent the entry of damaging substances. While the BBB plays an important role in CNS homeostasis, it also creates a bottleneck for the delivery of therapeutics (*1*–*3*). In addition, BBB dysfunction has been observed in many CNS pathologies, including Alzheimer's disease, multiple sclerosis, and stroke, and increasing evidence demonstrates that treating BBB contribution to CNS disorders may improve disease outcomes (*4*–*12*). BMECs gain their unique properties as a result of coordinated signaling cues from other brain cells surrounding CNS microvessels, including CNS pericytes, astrocytes, and neurons that together with BMECs form the neurovascular unit (NVU) (*13*–*18*). Recently, brain pericyte contributions to BBB development and function have begun to be elucidated, and potential pericyte roles in CNS disease have been suggested. CNS pericytes associate with BMECs early in embryonic development as nascent blood vessels invade the developing neural tube. The emergence of pericytes corresponds to BBB formation through reduction of transcytosis, decreased immune cell adhesion molecule expression, and reduced ultrastructural tight junction abnormalities (*13*). In the adult, pericytes regulate vascular stability and diameter (*5*, *19*–*21*), contribute to the BMEC basement membrane (*20*, *22*–*24*), regulate BMEC molecular phenotype (*14*, *25*), and reduce nonspecific molecular transcytosis (*14*).

As a result of the emerging importance of brain pericytes in brain health and disease, they have been increasingly incorporated into in vitro models of the BBB. For example, coculture with pericytes can improve BMEC phenotype in coculture systems, stabilize endothelial cell cord formation in vitro (*26*), and induce BMEC properties in primary and hematopoietic stem cell–derived endothelial cells (*27*–*29*). We also reported that primary brain pericytes could be combined with human pluripotent stem cell (hPSC)–derived BMECs and enhance their functionality (*30*). Such hPSC-derived BBB models offer the capability to screen for CNS-penetrant therapeutics (*31*) and can be used to investigate BBB contributions to human disease using patient-derived induced pluripotent stem cells (iPSCs) (*32*, *33*). While we and others have recently demonstrated the combination of iPSC-derived BMECs with iPSC-derived astrocytes and neurons to form high-fidelity multicellular BBB models (*34*–*36*), the inclusion of brain pericytes, to date, has largely been limited to primary human sources (*30*, *35*, *37*). Unfortunately, primary sources do not scale with high fidelity (*38*, *39*) and, unlike iPSC sources, do not reflect the genetic contributions that can be important to modeling human disease. Thus, for patient-specific modeling of the healthy and diseased BBB, it is paramount to generate brain pericyte–like cells from human iPSCs.

Vascular mural cells include both smooth muscle cells, which line arterioles and venules, and pericytes, which are associated with smaller microvessels and capillaries. Until very recently, it has been difficult to distinguish smooth muscle cells from pericytes based on marker expression (*40*). Moreover, hPSC-derived mural cells from different embryonic origins display functionally distinct phenotypes and respond differentially to disease pathways (*41*, *42*). While most mural cells originate from mesoderm, CNS forebrain mural cells arise from neural crest stem cells (NCSCs) (*43*, *44*), a multipotent stem cell population capable of forming peripheral neurons and mesenchymal derivatives, including adipocytes, osteocytes, and chondrocytes (*45*, *46*), among other cell types. Previous studies have described processes to differentiate hPSCs to NCSCs and demonstrated their potential to form vascular smooth muscle cells (*42*, *46*, *47*). However, it is unknown whether NCSCs can generate pericyte-like cells that enhance

[1]Department of Chemical and Biological Engineering, University of Wisconsin–Madison, Madison, WI, USA. [2]Department of Orthopedics and Rehabilitation, University of Wisconsin School of Medicine and Public Health, Madison, WI, USA. [3]Departments of Neuroscience and Pharmacology, University of California, San Diego, San Diego, CA, USA.
*Present address: Fujifilm Cellular Dynamics, Madison, WI, USA.
†These authors contributed equally to this work.
‡Present address: Department of Cellular and Integrative Physiology, Indiana University School of Medicine, Terre Haute, IN, USA.
§Present address: Ecolab Inc., 1 Ecolab Place, St. Paul, MN, USA.
‖Corresponding author. Email: eshusta@wisc.edu (E.V.S.); sppalecek@wisc.edu (S.P.P.)

BBB phenotypes in BMECs. Here, we describe a facile protocol for generating multipotent NCSCs from hPSCs by canonical WNT signaling activation with simultaneous inhibition of bone morphogenetic protein (BMP) and activin/nodal signaling as previously described (*46*, *48*). These hPSC-derived NCSCs can be further differentiated to mural cells that express pericyte markers by 9 days of culture in serum-containing medium. These pericyte-like cells associated with vascular cord networks and induced key pericyte-driven phenotypes in BMECs, including the enhancement of barrier properties and reduction of transcytosis. Last, an isogenic model of the NVU composed of iPSC-derived pericytes, BMECs, astrocytes, and neurons exhibited elevated barrier properties compared to a model lacking pericytes, suggesting future applications of iPSC-derived pericytes in CNS drug screening, BBB development studies, and disease modeling applications.

RESULTS

Directed differentiation of hPSCs to NCSCs in low-protein medium

We first assessed the capability of E6, a reduced-factor medium, to support differentiation of H9 human embryonic stem cells (hESCs) and IMR90C4 and CS03n2 iPSCs to NCSCs. H9 hESCs were cultured for 15 days in E6 medium supplemented with heparin and pathway modulators previously implicated in hPSC differentiation to NCSCs (*48*): 1 μM CHIR99021 (a glycogen synthase kinase-3β inhibitor to promote WNT signaling), 10 μM SB431543, [an activin receptor-like kinase 5 antagonist to inhibit activin/nodal/transforming growth factor–β (TGFβ) signaling], and 10 ng/ml fibroblast growth factor 2 (FGF2) (E6-CSF). However, E6-CSF failed to produce p75-NGFR$^+$/HNK1$^+$ NCSCs, and increasing CHIR99021 concentration (2 μM) did not aid in inducing p75-NGFR (nerve growth factor receptor) expression (fig. S1A).

BMP signaling during hPSC differentiation to NCSCs can inhibit NCSC formation, and WNT signaling activation can induce downstream BMP signaling in hPSCs (*46*); however, the requirement of BMP inhibition in NCSC differentiation has been variable (*42*, *46*). To examine the effects of BMP inhibition on hPSC differentiation to NCSCs in minimal medium, E6-CSF medium was supplemented with 1 μM dorsomorphin, a BMP type I receptor inhibitor, to generate E6-CSFD. With BMP inhibition, H9 hESCs progressed to p75-NGFR$^+$/HNK1$^+$ NCSCs that also expressed activating enhancer-binding protein-2 (AP-2) after 15 days of E6-CSFD treatment (Fig. 1, A to C and J, and fig. S1, D and E). E6-CSFD also drove NCSC formation in IMR90C4 and CS03n2 iPSC lines (Fig. 1J and fig. S1, B to E). H9 and CS03n2 hPSCs yielded cultures comprising ~90% NCSCs, while purity of IMR90C4-derived NCSCs was frequently lower (Fig. 1J). Temporal mRNA analysis confirmed loss of pluripotency by day 15 (D15) of E6-CSFD treatment, as indicated by loss of *NANOG* and *POU5F1* pluripotency transcripts (Fig. 1D and fig. S1F). In addition, after 15 days of E6-CSFD treatment, the differentiation mixture expressed NCSC-associated transcripts, including *TFAP2A*, *SOX9*, *SOX10*, *B3GAT1* (HNK1), and *NGFR* (Fig. 1D and fig. S1F). At D15 of E6-CSFD treatment, cells had undergone approximately seven population doublings (Fig. 1E), corresponding to over 100 NCSCs per input hPSC.

To purify NCSCs from the differentiation cultures, D15 NCSCs were positively selected using anti–p75-NGFR magnetic-activated cell sorting (MACS). MACS enriched p75-NGFR$^+$/HNK1$^+$ NCSC populations above 95% for all three hPSC lines tested (Fig. 1, F and J, and fig. S1, G and H). Sorted NCSCs retained p75-NGFR and HNK1 expression following replating (Fig. 1G). In addition, treating NCSCs with N2 medium supplemented with brain-derived neurotrophic factor (BDNF), glial cell line–derived neurotrophic factor (GDNF), neurotrophin-3 (NT-3), and nerve growth factor-β (NGF-β) yielded βIII-tubulin$^+$/peripherin$^+$ peripheral neurons (Fig. 1H and fig. S1I). We additionally expanded sorted NCSCs for 11 days and then differentiated these cells to mesenchymal derivatives: Oil Red O$^+$ adipocytes were obtained by treating NCSCs with insulin, 3-isobutyl-1-methylxanthine (IBMX), and dexamethasone; Alcian blue$^+$ chondrocytes were obtained using pellet culture and TGFβ1-containing chondrogenic medium; and Alizarin red$^+$ osteocytes were obtained using dexamethasone, glycerophosphate, and ascorbic acid (Fig. 1I and fig. S1J). Together, these data demonstrate that the reduced-factor, low-protein E6-CSFD medium directs hPSCs to NCSCs over a 15-day differentiation period and that MACS-purified NCSCs retain the potential to form NCSC derivatives.

Serum treatment directs hPSC-derived NCSCs to mural cell lineages

We subsequently identified differentiation conditions capable of driving NCSCs to mural cell lineages (Fig. 2A), as defined by co-expression of platelet-derived growth factor receptor β (PDGFRβ) and neuron-glial antigen 2 (NG2) (*40*, *49*). PDGFRβ was expressed in D15 NCSCs (Fig. 2C) and in replated cells 1 day following MACS (D16), but NG2 expression was absent in both of these cell populations (Fig. 2, C and F). Given the importance of PDGF-BB and TGFβ1 in mural cell development (*50*, *51*), we first tested whether these factors could induce NG2 expression in NCSCs while also maintaining PDGFRβ expression. NCSCs cultured for 6 days in E6 medium generated cells that were PDGFRβ$^+$, but NG2 expression was not observed (Fig. 2B). Supplementation of E6 medium with PDGF-BB and TGFβ1 did not induce NG2 expression. However, when E6 medium was supplemented with 10% fetal bovine serum (FBS), resultant cells expressed both PDGFRβ and NG2 (Fig. 2B). Comparing differentiation in E6 + 10% FBS on uncoated tissue culture polystyrene (TCPS) to gelatin-coated TCPS, which has previously been reported as conducive to mural cell differentiation (*52*), the uncoated substrate yielded a qualitatively larger fraction of cells that expressed PDGFRβ and NG2 (Fig. 2B). Given the capacity for E6 + 10% FBS on uncoated substrate to direct hPSC-derived NCSCs to PDGFRβ$^+$/NG2$^+$ mural cells, we further evaluated these cells.

The temporal evolution of hPSC-derived NCSCs to PDGFRβ$^+$/NG2$^+$ mural cells using E6 + 10% FBS was examined over a 9-day period (D16 to D25). At D15 of differentiation, 92.4 ± 1.1% of H9-derived NCSCs expressed PDGFRβ, and after 9 days of serum treatment, nearly all cells were PDGFRβ$^+$ (99.6 ± 0.2%) (Fig. 2, C and D), with expression of the *PDGFRB* transcript present in D15 NCSCs and throughout the differentiation in serum (Fig. 2E). In contrast, despite the fact that the NG2-encoding *CSPG4* transcript was expressed in D15 NCSCs (Fig. 2E), NG2 protein was not detected at this time point by flow cytometry (Fig. 2C). However, the percentage of cells expressing NG2 increased over the 9-day differentiation period, with nearly all cells becoming NG2$^+$ (99.4 ± 0.3% at D25; $P <$ 0.05 versus D15) (Fig. 2, C and D). The E6 + 10% FBS differentiation scheme also generated at least ~90% PDGFRβ$^+$ and NG2$^+$ cells in IMR90C4- and CS03n2-derived NCSCs following 9 days of E6 + 10% FBS treatment (D25; Fig. 1J and fig. S2, A to D). At D22, this procedure yielded a roughly 10-fold expansion in mural cells (9.5 ± 1.3 mural cells per sorted NCSC for six independent differentiations).

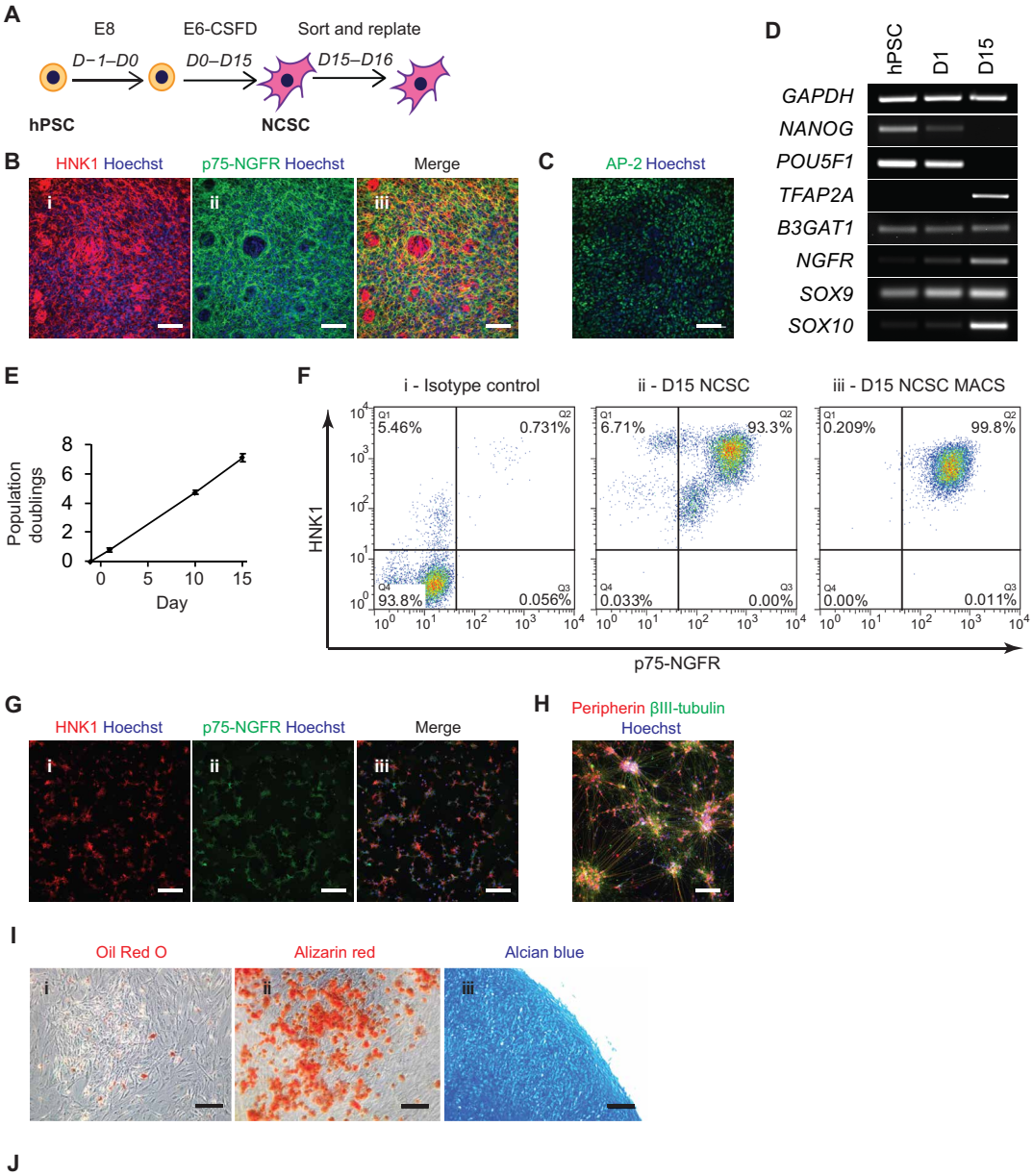

J

Cell line	D15 NCSC			D15 NCSC MACS		D25 pericyte-like cells		
	n	% p75-NGFR$^+$ HNK1$^+$	% p75-NGFR$^+$ HNK1$^-$	*n*	% p75-NGFR$^+$ HNK1$^+$	*n*	% NG2$^+$	% PDGFRβ$^+$
H9	13	87.5 ± 11.3	2.5 ± 3.7	9	98.2 ± 2.6	3	99.4 ± 0.4	99.6 ± 0.3
IMR90C4	13	64.0 ± 37.1	1.8 ± 3.9	7	95.0 ± 4.4	3	89.3 ± 11.8	93.3 ± 1.5
CS03n2	6	90.3 ± 7.8	1.0 ± 1.2	6	96.5 ± 2.8	3	94.0 ± 4.6	95.2 ± 3.2

Fig. 1. Generation of multipotent NCSC populations. (**A**) NCSC differentiation timeline. Small-molecule activation of canonical WNT signaling and small-molecule inhibition of activin/nodal/TGFβ/BMP signaling in minimal medium produce H9-derived NCSCs over a 15-day treatment window. NCSCs are then magnetically sorted and replated for subsequent mural cell differentiation. (**B**) Immunocytochemistry images of H9 hESCs differentiated in E6-CSFD probed for the presence of HNK1 and p75-NGFR at D15. NCSCs are HNK1$^+$/p75-NGFR$^+$ cells. Hoechst nuclear counterstain (blue) is also included. Scale bars, 100 μm. (**C**) AP-2 immunocytochemistry images for H9-derived NCSCs at D15. Hoechst nuclear counterstain (blue) is also included. Scale bar, 100 μm. (**D**) Temporal polymerase chain reaction (PCR) analysis of pluripotency (*NANOG* and *POU5F1*) and NCSC (*TFAP2A*, *B3GAT1*, *NGFR*, *SOX9*, and *SOX10*) transcripts. (**E**) Quantification of NCSC expansion in population doublings over the 15 days of NCSC differentiation. Plotted are the means ± SD of three technical replicates of a representative differentiation. (**F**) Flow cytometry analysis of H9-derived NCSCs. Panels include isotype controls (i), NCSC (HNK1$^+$/p75-NGFR$^+$) purity before magnetic-activated cell sorting (MACS) (ii), and NCSC purity following MACS (iii). Inset percentages are included in each quadrant. Quantitation is shown in (J). (**G**) Immunocytochemistry analysis of D16 NCSCs following MACS and replating. NCSCs maintained HNK1 and p75-NGFR expression. Hoechst nuclear counterstain (blue) is also included. Scale bars, 100 μm. (**H**) Immunocytochemistry analysis of H9-derived NCSCs subsequently differentiated in peripheral neuron medium. Resultant cells were positive for βIII-tubulin and peripherin expression. Hoechst nuclear counterstain (blue) is also included. Scale bar, 200 μm. (**I**) H9-derived NCSCs could be differentiated into mesenchymal derivatives, including Oil Red O–stained adipocytes (i, red), Alizarin red–stained osteocytes (ii, red), and Alcian blue–stained chondrocytes (ii, blue). Scale bars, 200 μm. (**J**) NCSC and pericyte-like cell differentiation efficiencies for three hPSC lines.

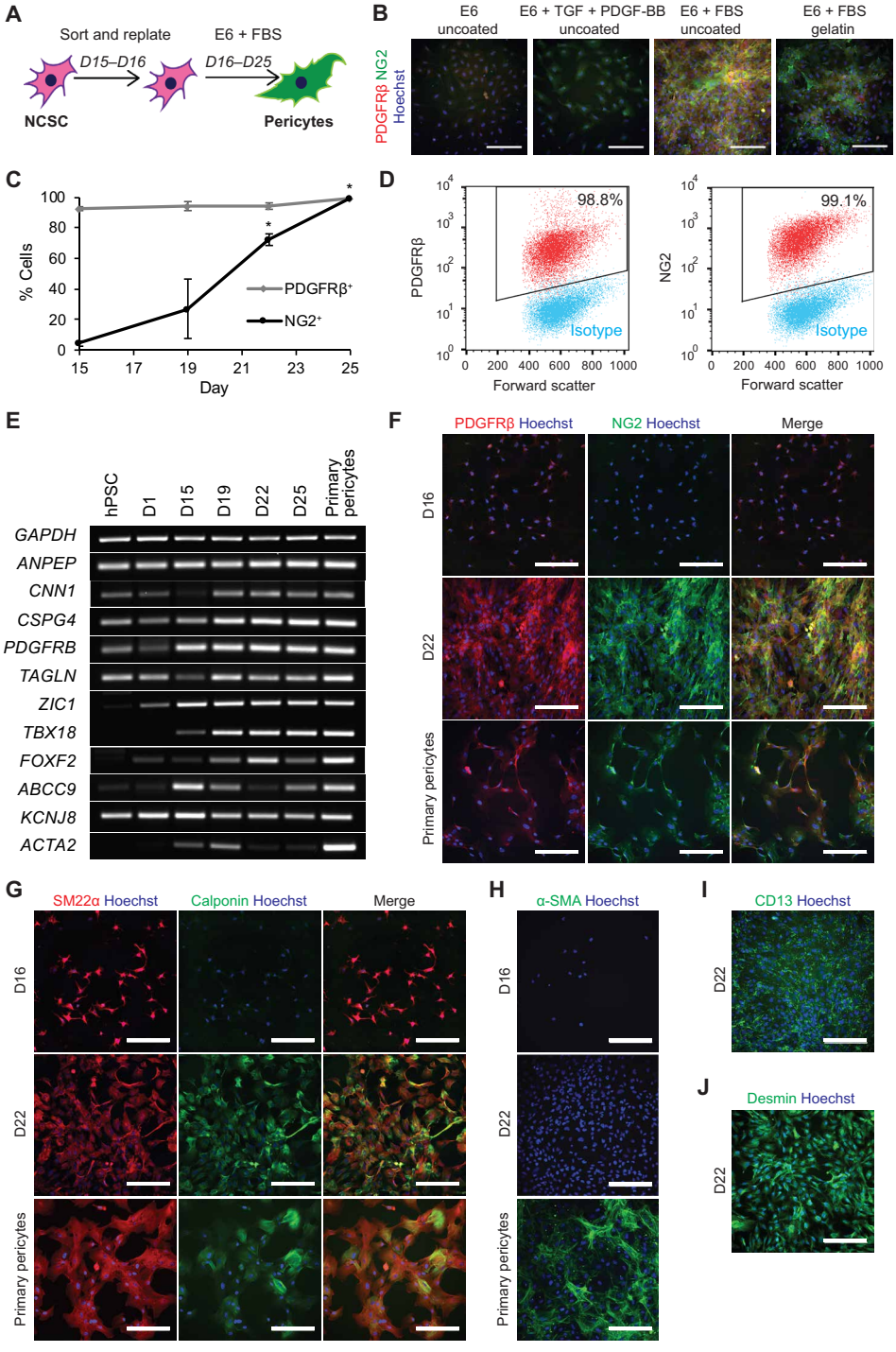

Fig. 2. Serum treatment directs H9-derived NCSCs toward mural cells. (**A**) Differentiation timeline for mural cell differentiation. Replated NCSCs are differentiated to mural cells in E6 medium + 10% FBS for 9 days. (**B**) PDGFRβ and NG2 immunocytochemistry of cells obtained after treating replated H9-derived NCSCs for 6 days in E6, E6 + TGFβ1 + PDGF-BB, or E6 + 10% FBS on uncoated tissue culture polystyrene or E6 + 10% FBS on gelatin-coated tissue culture polystyrene. Scale bars, 200 μm. (**C**) Temporal flow cytometry analysis for PDGFRβ$^+$ and NG2$^+$ cells in H9-derived NCSCs treated with E6 + 10% FBS. Depicted are the means ± SEM of at least two independent differentiations at each time point, *P < 0.05 versus D15 NCSCs using analysis of variance (ANOVA) followed by Dunnett's test. (**D**) Representative PDGFRβ and NG2 flow cytometry plots for H9-derived NCSCs treated for 9 days with E6 + 10% FBS medium. Quantitative data can be found in Fig. 1J. (**E**) Temporal PCR analysis of mural and pericyte transcripts for the differentiating H9 hESCs. (**F**) PDGFRβ and NG2 immunocytochemistry of H9-derived NCSCs (D16), mural cells (D22), and primary pericytes. Hoechst nuclear counterstain (blue) is also included. Scale bars, 200 μm. (**G**) Calponin and SM22α immunocytochemistry of H9-derived NCSCs (D16), mural cells (D22), and primary pericytes. Hoechst nuclear counterstain (blue) is also included. Scale bars, 200 μm. (**H**) α-SMA immunocytochemistry of H9-derived NCSCs (D16), mural cells (D22), and primary pericytes. Hoechst nuclear counterstain (blue) is also included. Scale bars, 200 μm. (**I**) CD13 immunocytochemistry of H9-derived mural cells (D22). Hoechst nuclear counterstain (blue) is also included. Scale bar, 200 μm. (**J**) Desmin immunocytochemistry of H9-derived mural cells (D22). Hoechst nuclear counterstain (blue) is also included. Scale bar, 200 μm.

To further probe the transition of hPSC-derived NCSCs to pericyte-like cells, we examined the temporal evolution of transcripts that have been associated with pericytes and other mural cells. H9 hESCs expressed *CNN1* (calponin) and *TAGLN* (SM22α), which encode contractile proteins implicated in early mural cell differentiation (*41*), as did NCSCs and mural cells (Fig. 2E). At D16, replated hPSC-derived NCSCs expressed SM22α, but calponin expression was not observed (Fig. 2G and fig. S2, F and K). By D22, differentiating hPSC-derived NCSCs exhibited calponin/SM22α coexpression with cellular localization to contractile fibers (Fig. 2G and fig. S2, F and K). α–Smooth muscle actin (α-SMA) was not detected in D22 cells treated with E6 + 10% FBS, although serum transiently increased abundance of the transcript (*ACTA2*) before down-regulation (Fig. 2, E and H, and figs. S2, G and L, and S3F). In contrast, NCSCs treated with E6 alone or E6 + PDGF-BB and TGFβ1 expressed α-SMA in addition to calponin and SM22α (fig. S3, A and B). In addition, these cells exhibited a morphology similar to that of smooth muscle cells, with large cell bodies and distinct cell borders, whereas the cells differentiated in E6 + 10% FBS were smaller, with numerous projections reminiscent of cultured primary brain pericytes (Fig. 2, G and H). After extended culture in E6 + 10% FBS (D45), the resultant cells continued to be $PDGFR\beta^+/NG2^+$ and expressed calponin and SM22α, while α-SMA was still absent (fig. S3, C to E). Primary human brain pericytes expressed all three contractile proteins and had a morphology similar to that of the serum-treated NCSC-derived mural cells (Fig. 2, F to H). CD13 and desmin were expressed in both D16 NCSCs and D22 mural cells, while primary brain pericytes expressed desmin, but CD13 expression was weak (Fig. 2, I and J, and fig. S2, H, I, and M to R).

Additional transcript analysis was used to further characterize the differentiation process. The mural cell marker, *ANPEP* (CD13), was expressed throughout the differentiation process. While *PDGFRB*, *CSPG4* (NG2), *CNN1*, *TAGLN*, *ANPEP*, and *TBX18* are mural cell markers expressed throughout the body, *FOXF2* and *ZIC1* have been suggested as being selectively expressed in brain mural cells (*53*–*55*). Accordingly, given the NCSC origin of the mural cells, *FOXF2* and *ZIC1* were induced during the differentiation (Fig. 2E and fig. S3F). Until recently, it has been difficult to use markers to distinguish pericytes from smooth muscle cells in the brain; however, it has been suggested that *ABCC9* and *KCNJ8* are two transcripts having selective expression in brain pericytes as compared to smooth muscle (*40*, *49*). *ABCC9* levels were biphasic with strong expression in D15 NCSCs and then a reinduction in D25 mural cells. *KCNJ8* was expressed fairly uniformly throughout the differentiation process (Fig. 2E). Similar results were observed for mural cells derived from IMR90C4- and CS03n2-derived NCSCs, although the IMR90C4 mural cells had weaker *ZIC1* and *ABCC9* signatures (fig. S3F). Overall, the transcript profile of mural and pericyte-associated genes in the NCSC-derived mural cells was qualitatively very similar to that of primary human brain pericytes (Fig. 2E).

We next used RNA sequencing (RNA-seq) to quantify global gene expression in NCSC-derived mural cells and to evaluate the temporal emergence of a pericyte-like population. As expected, unbiased hierarchical clustering based on expression [fragments per kilobase of transcript per million mapped reads (FPKM)] of all transcripts revealed the highest similarity between NCSC-derived mural cells generated from three independent differentiations from H9 hESCs and the two differentiations from IMR90C4 and CS03n2 iPSCs (Fig. 3A, D25 sample cluster). The Pearson correlation coefficients comparing transcript expression in H9-derived mural cells at D25 to the two replicate H9 differentiations were 0.99 and 0.98 (D25 H9-A versus D25 H9-B or H9-C; $P < 0.0001$). Moreover, the Pearson correlation coefficients comparing the mural cells derived from the H9 hESC line to those derived from IMR90C4 and CS03n2 iPSCs were both 0.97 (D25 H9-A versus D25 IMR90 or CS03; $P < 0.0001$). Collectively, these data indicate a highly reproducible differentiation procedure among replicated differentiations and hPSC lines. Furthermore, NCSC-derived mural cells at D25 clustered more closely with primary brain pericytes than with D15 NCSCs, D55 NCSCs that had been maintained in E6-CSFD following MACS, or hPSCs (Fig. 3A). The Pearson correlation coefficient between the average transcript expression of all D25 NCSC-derived mural cell samples and the average of the primary pericyte samples was 0.89 ($P < 0.0001$), suggesting strong positive association between NCSC-derived mural cells and primary human pericytes. Consistent with reverse transcription polymerase chain reaction (RT-PCR) experiments (Figs. 1D and 2E), temporal analysis of transcript expression demonstrated down-regulation of pluripotency markers *NANOG* and *POU5F1* and transient up-regulation of *NGFR*, *B3GAT1*, *SOX9*, and *SOX10*, as well as the cranial neural crest marker *ETS1*, in D15 NCSCs (Fig. 3B). We also observed gradual induction of *CSPG4*, *PDGFRB*, *CNN1*, *TAGLN*, *ANPEP*, *TBX18*, *ABCC9*, and *KCNJ8* over the time course of E6 + 10% FBS treatment and transient up-regulation of *ACTA2*, *DES*, *ADGRA2* (GPR124), and *FOXF2* (Fig. 3B). Expression levels of *CSPG4*, *PDGFRB*, *CNN1*, *TAGLN*, *FOXF2*, *ABCC9*, *KCNJ8*, *DES*, and *ADGRA2* were similar to those of NCSC-derived mural cells and primary brain pericytes; however, consistent with the lack of α-SMA expression (Fig. 2H and fig. S2, G and L), NCSC-derived mural cells expressed nearly 100-fold less *ACTA2* transcript than primary pericytes (Fig. 3B). By D45, NCSC-derived mural cells retained expression of most markers at levels similar to that of D25 cells, while *ANPEP*, *ABCC9*, and *KCNJ8* expression further increased, suggesting that these cells may continue to mature during extended culture in E6 + 10% FBS (Fig. 3B). Analysis of transcripts up-regulated in NCSC-derived mural cells compared to their NCSC precursors revealed several enriched Gene Ontology (GO) terms, including vascular development, blood vessel morphogenesis, and extracellular matrix organization (Fig. 3C), indicating that differentiation drives the progression from NCSCs to mural cells with vascular-associated transcript signatures. Of the 46 genes with human homologs identified as pericyte-enriched by single-cell RNA-seq in mice (*40*), 29 were expressed at or above 1 FPKM by NCSC-derived mural cells and 26 were expressed by primary pericytes (Fig. 3D and table S2). Last, NCSCs maintained in E6-CSFD retained neural crest marker expression and did not develop expression of pericyte markers (fig. S6). Collectively, these data demonstrate that differentiation of NCSCs in E6 + 10% FBS yielded a mural cell population that expressed pericyte-associated markers while closely mimicking primary brain pericytes at a transcriptome level. Thus, we refer to the NCSC-derived mural cells as brain pericyte–like cells throughout the remainder of the manuscript.

Brain pericyte–like cells assemble with vascular cord networks

Pericytes associate with endothelial cells and stabilize nascent vascular networks (*51*). To assess the ability of brain pericyte–like cells to self-assemble with endothelial cells, an in vitro endothelial cord forming assay was performed. A 3:1 mixture of primary pericytes or hPSC-derived brain pericyte–like cells (D22) and human umbilical

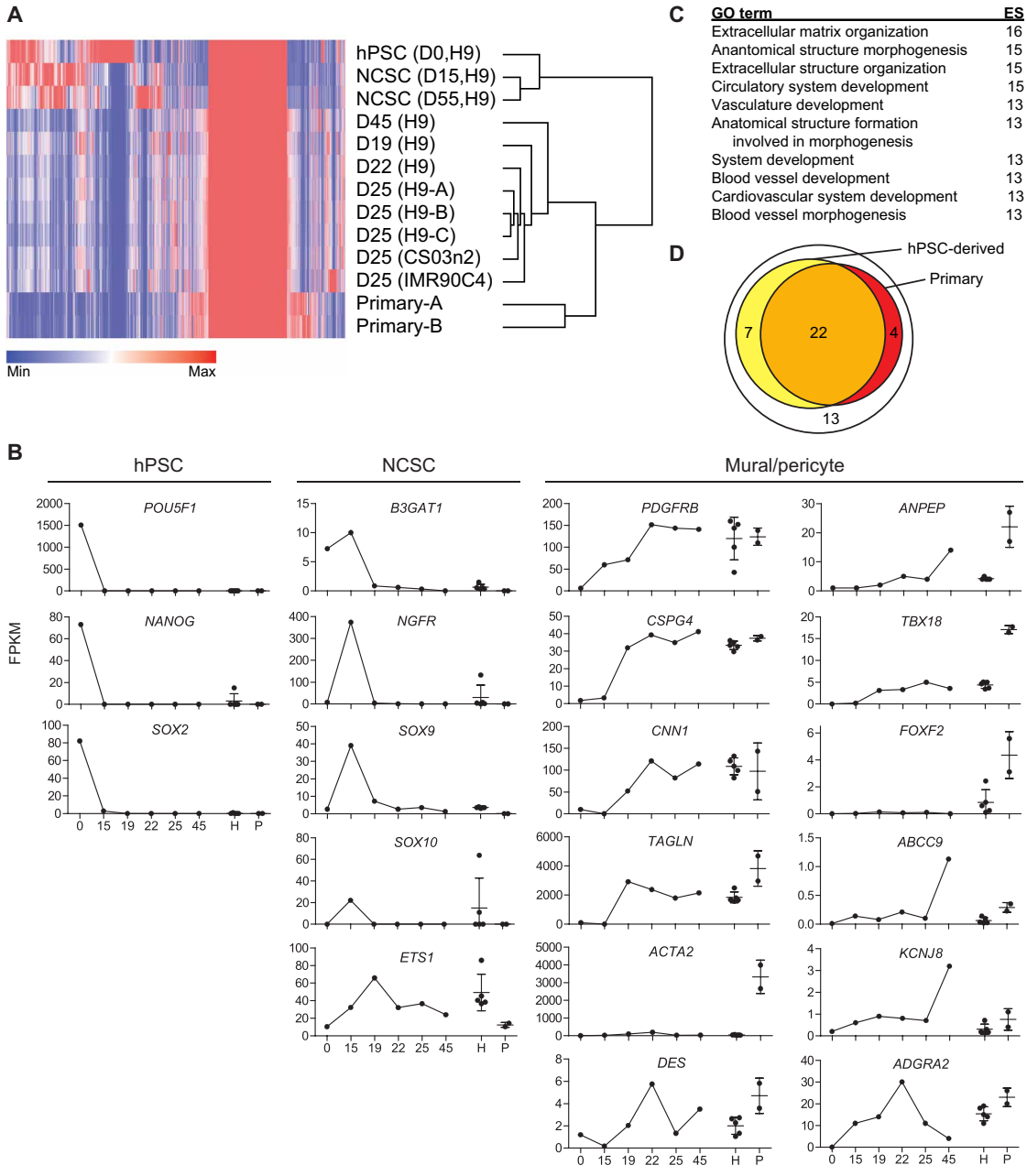

Fig. 3. RNA-seq of pericyte-like cells and related cell types. (**A**) Hierarchical clustering based on all transcripts of undifferentiated H9 hESCs; H9-derived NCSCs at D15 and after an additional 40 days in E6-CSFD (D55); H9-derived pericyte-like cells at D19, D22, and D25 (three independent differentiations at the D25 time point, indicated as "H9-A," "H9-B," and "H9-C"); H9-derived pericyte-like cells maintained for an additional 20 days in E6 + 10% FBS (D45); CS03n2- and IMR90C4-derived pericyte-like cells at D25; and primary brain pericytes (from two distinct cultures of the same cell source, indicated as "Primary-A" and "Primary-B"). (**B**) Expression (FPKM) of selected transcripts in H9 hPSCs (day "0"), NCSCs ("15"), and during the differentiation of pericyte-like cells ("19," "22," "25," and "45"). The mean transcript expression in all D25 hPSC-derived pericyte-like cells (H9-A to H9-C, CS03n2, and IMR90C4; "H") and in primary brain pericytes ("P") is also shown. Error bars represent SEM of five independent differentiations ("H") or of two primary pericyte samples ("P"). (**C**) Top 10 GO terms sorted by enrichment score [ES = $-\log_{10}$(FDR)] for hPSC-derived pericyte-like cells. Genes included in the dataset were enriched in pericyte-like cells (average of all D25 samples) compared to NCSCs (average of D15 and D55 samples) ($FPKM_{pericyte\text{-}like\ cells}/FPKM_{NCSC} \geq 10$) and were expressed at ≥1 FPKM in pericyte-like cells. (**D**) Expression (≥1 FPKM) of murine pericyte-enriched transcripts [46 transcripts (*40*)] in hPSC-derived pericyte-like cells (29 transcripts) and primary brain pericytes (26 transcripts). A detailed listing of genes and FPKM values can be found in table S2.

vein endothelial cells (HUVECs) or immortalized human BMECs (hBMECs) was plated on Matrigel (Fig. 4A and fig. S7A). H9-, CS03n2-, and IMR90C4-derived brain pericyte–like cells self-associated with HUVECs and hBMECs, much like primary human brain pericytes (Fig. 4, B and C, and fig. S7, B and C). After 24 hours, hPSC-derived pericyte-like cells exhibited high NG2 expression and aligned along the $CD31^+$ endothelial cell cord perimeter and developed pericyte-like morphology with stellate-shaped bodies and extended cell processes (Fig. 4, B and C). Whereas HUVECs or hBMECs alone and HUVECs or hBMECs in coculture with control human embryonic

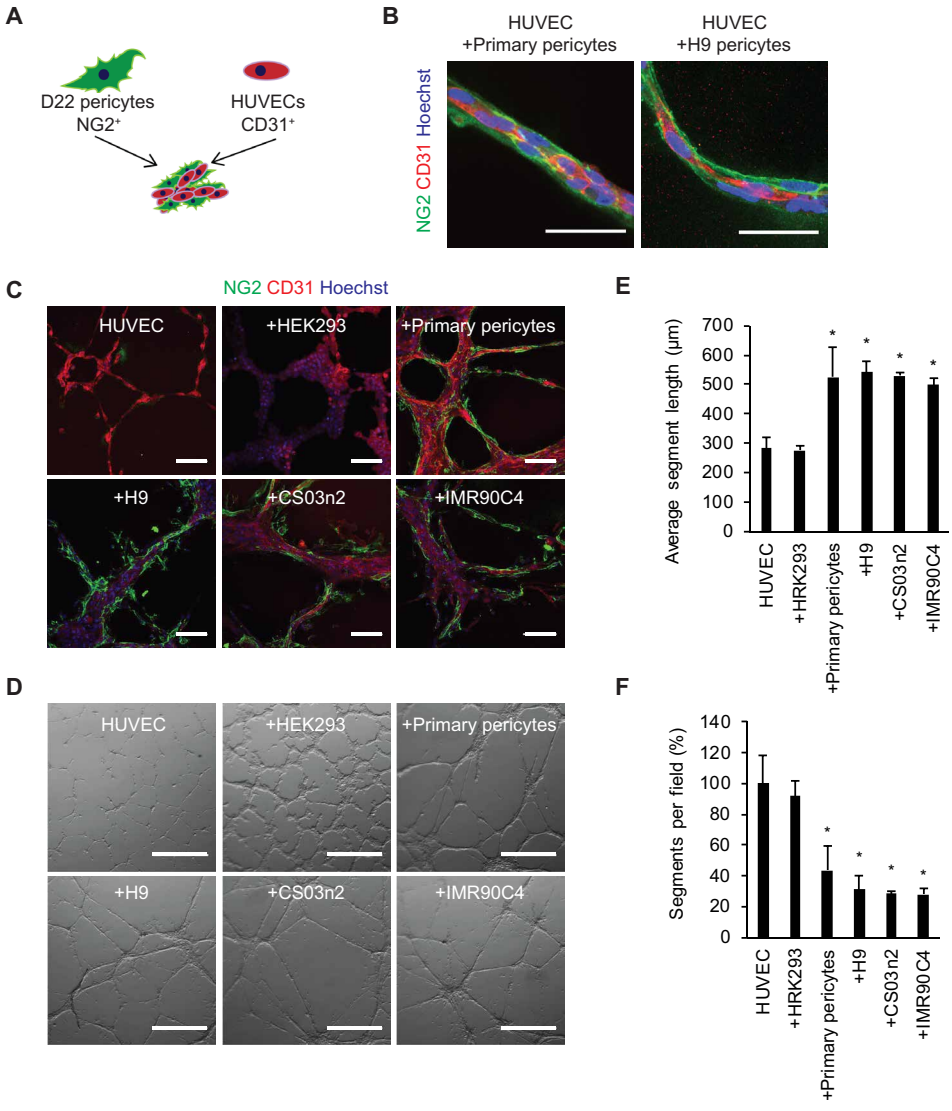

Fig. 4. hPSC-derived pericyte-like cell assembly with endothelial cells. (**A**) Self-assembly schematic. hPSC-derived pericyte-like cells self-assemble with HUVECs to form vascular cords. (**B**) Confocal immunocytochemistry images of primary pericytes and H9-derived pericyte-like cells (NG2) aligning with and extending processes along HUVEC cords (CD31). Hoechst nuclear counterstain (blue) is also included. Scale bars, 50 μm. (**C**) Immunocytochemistry images of HUVECs alone or cultured with HEK293 fibroblasts (+HEK293), primary human brain pericytes (+Primary pericytes), CS03n2-derived pericyte-like cells (+CS03n2), H9-derived pericyte-like cells (+H9), or IMR90C4-derived pericyte-like cells (+IMR90C4). Hoechst nuclear counterstain (blue) is also included. Scale bars, 100 μm. (**D**) Representative bright-field images of HUVECs alone or cultured with the various cell types. Scale bars, 300 μm. (**E**) Quantification of the average segment lengths from bright-field images in (D). Plotted are means ± SEM of three independent pericyte-like cell differentiations. *$P < 0.05$ versus HUVEC monoculture, ANOVA followed by Dunnett's test. (**F**) Quantification of the number of segments per field normalized to HUVEC monoculture from bright-field images in (D). Plotted are means ± SEM of three independent pericyte-like cell differentiations. *$P < 0.05$ versus HUVEC monoculture, ANOVA followed by Dunnett's test.

kidney–293 (HEK293) cells yielded many small branching cords, coculture with the hPSC-derived brain pericyte–like cells or primary human brain pericytes yielded fewer, appreciably longer cords (Fig. 4, C to F, and fig. S7, C to F). These data demonstrate that hPSC-derived NCSC lineage mural cells exhibit pericyte-like association, with endothelial cells leading to the formation of more well-developed cord networks.

Brain pericyte–like cells induce BBB properties

To investigate whether hPSC-derived brain pericyte–like cells can recapitulate key BBB-inducing properties that have been observed in vivo such as reduction in tight junction abnormalities and transcytosis, we next cocultured the pericyte-like cells with hPSC-derived BMECs generated as we previously described (*56*). When D22 brain pericyte–like cells were cocultured with hPSC-derived BMECs, the BMEC barrier properties as measured by transendothelial electrical resistance (TEER) were substantially elevated, while coculture with a noninducing cell type (3T3) yielded no barrier enhancement (Fig. 5, A and B). TEER elevation by hPSC-derived brain pericyte–like cells was indistinguishable from that induced by primary human brain pericytes (Fig. 5B). The TEER increases were accompanied by a corresponding decrease in permeability to fluorescein, a hydrophilic small-molecule tracer (Fig. 5C). After BMEC coculture, the brain pericyte–like cells remained $NG2^+/PDGFR\beta^+$ (fig. S4A), indicating their continued maintenance of mural identity. To determine tight

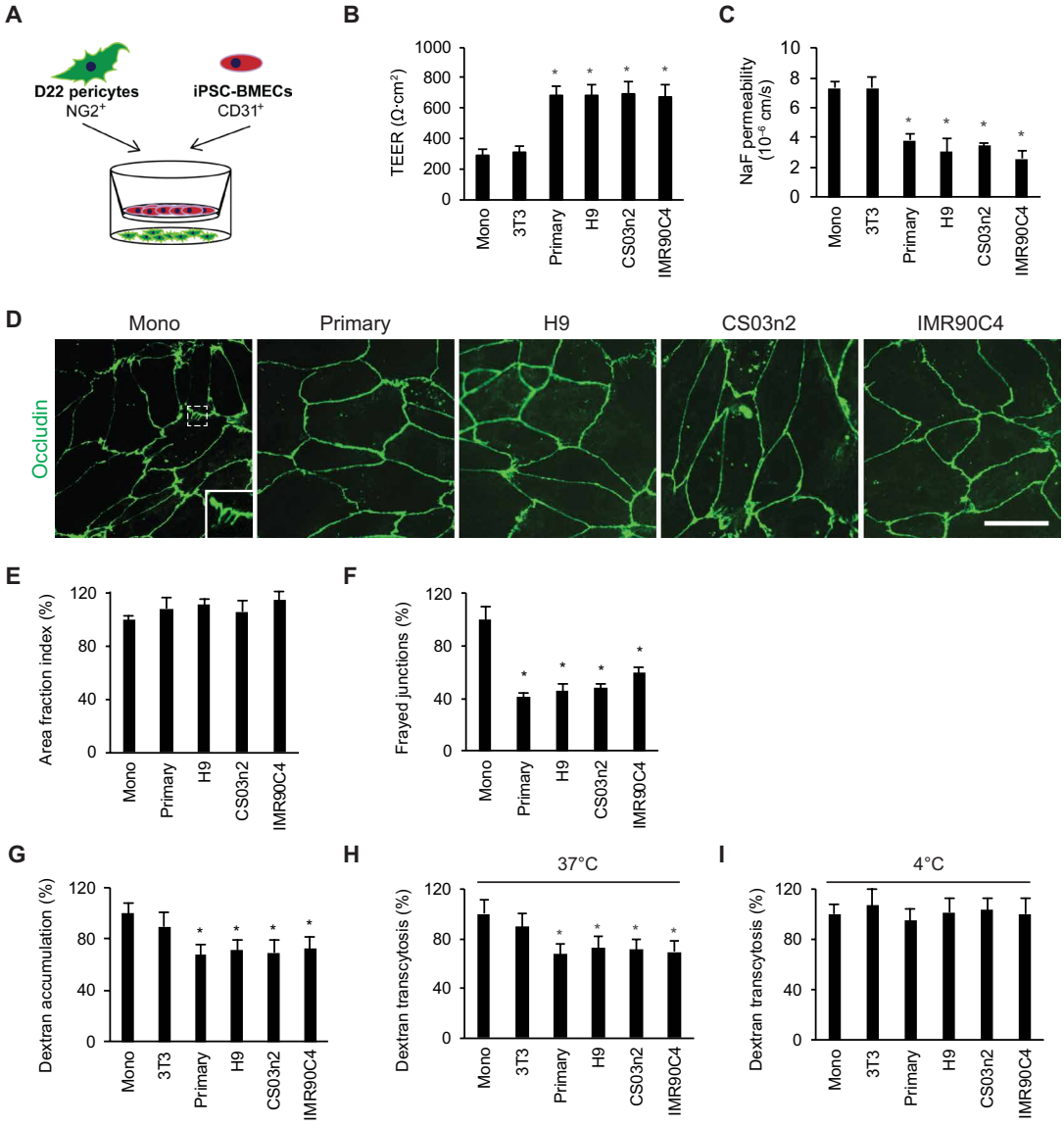

Fig. 5. Measurement of the effects of hPSC-derived pericyte-like cells on BBB phenotypes. (**A**) Schematic of Transwell setup for coculture assays. (**B**) Maximum TEER achieved by IMR90C4-derived BMEC monoculture or coculture with 3T3 mouse fibroblasts, primary human brain pericytes, H9-derived pericyte-like cells, CS03n2-derived pericyte-like cells, or IMR90C4-derived pericyte-like cells. Plotted are the means ± SEM of at least three independent differentiations per condition. *$P < 0.05$ versus monoculture, ANOVA followed by Dunnett's test. (**C**) Sodium fluorescein permeability for IMR90C4-derived BMECs in monoculture or coculture with cell types as described in (B). Plotted are the means ± SEM of at least three independent differentiations per condition. *$P < 0.05$ versus monoculture, ANOVA followed by Dunnett's test. (**D**) Representative images of occludin immunocytochemistry of BMECs cultured for 48 hours in EC medium (Mono) or EC medium conditioned by the cell types described in (B). Enlarged example of a frayed junction is inset in the monoculture panel. Scale bar, 25 μm. (**E**) Quantification of occludin area fraction index for the samples described in (D). Plotted are the means ± SEM of three independent differentiations. No significant difference by ANOVA. (**F**) Quantification of frayed junctions visualized by occludin immunocytochemistry for the samples described in (D). Plotted are the means ± SEM of three independent differentiations. *$P < 0.05$ versus monoculture, ANOVA followed by Dunnett's test. (**G**) Accumulation of Alexa 488–tagged 10-kDa dextran in IMR90C4-derived BMECs following 48 hours of coculture with cell types as described in (B). All results are normalized to BMEC monoculture control. Plotted are the means ± SD of three Transwells. Results are representative of three independent differentiations. *$P < 0.05$ versus monoculture, ANOVA followed by Dunnett's test. (**H** and **I**) Transcytosis of Alexa 488–tagged 10-kDa dextran at 37°C (H) or 4°C (I) across IMR90C4-derived BMECs following 48 hours of coculture with the cell types as described in (B). All results are normalized to BMEC monoculture control. Plotted are the means ± SD from three Transwells. Results are representative of three independent differentiations. *$P < 0.05$ versus monoculture, ANOVA followed by Dunnett's test. No significant differences at 4°C by ANOVA.

junction changes that may drive the induction in BMEC barrier properties, the expression level and localization of tight junction proteins occludin and claudin-5 were evaluated in the BMECs. Expression levels of occludin and claudin-5 were unchanged by coculture (fig. S4B). In addition, quantitative immunocytochemical evaluation of occludin and claudin-5 indicated that the number of cells having continuous tight junctions was unchanged upon treatment with pericyte-conditioned medium (Fig. 5, D and E, and fig. S4C). However, the

percentage of cells with occludin tight junction abnormalities or fraying was substantially reduced by treatment with pericyte-conditioned medium (Fig. 5F), correlating with the reduced permeability, while claudin-5 fraying remained unchanged (fig. S4C).

Next, the effects of brain pericyte–like cell coculture on BMEC transcytosis properties were evaluated. To test nonspecific molecular uptake and transcytosis in BMECs, 10-kDa Alexa 488–tagged dextran was dosed into the apical Transwell chamber, and accumulation into and transcytosis across the BMEC monolayer were quantified. After BMEC culture with medium conditioned by hPSC-derived brain pericyte–like cells, confocal imaging indicated a qualitative decrease in intracellular dextran uptake in punctate vesicular structures, similar to that observed with primary human brain pericytes, whereas medium conditioned by 3T3 control cells had no effect (fig. S4D). Quantification of dextran accumulation in BMECs cocultured with brain pericyte–like cells or primary brain pericytes indicated that BMEC accumulation was reduced by about 30% (Fig. 5G). These differences in accumulation translated to a corresponding 30% decrease in 10-kDa dextran transcytosis upon pericyte coculture (Fig. 5H). In contrast, when 10-kDa dextran transport was measured at 4°C, conditions that inhibit vesicular transcytosis processes, pericyte coculture did not affect dextran transport compared to 3T3s or hPSC-derived BMEC monoculture (Fig. 5I), indicating that the observed decreases in dextran transport could not be ascribed to differences in paracellular transport resulting from improved tight junction fidelity.

Last, to confirm that the effects of hPSC-derived brain pericyte–like cells are not specific to BMECs derived from hPSCs, the induction of BBB and transcytosis attributes was also evaluated in primary rat BMECs. Coculture with IMR90C4-derived brain pericyte–like cells elevated the TEER in primary rat BMECs to the same level as observed with primary human brain pericytes (fig. S5A). In addition, coculture with brain pericyte–like cells also reduced accumulation and transcytosis of 10-kDa dextran in primary rat BMECs (fig. S5, B and C). In summary, these data indicate that hPSC-derived brain pericyte–like cells can induce BBB phenotypes, including elevation of BMEC barrier tightness and reduction in transcytosis.

iPSC-derived brain pericyte–like cells can be integrated into an isogenic NVU model

Previously, we demonstrated that sequential coculture of iPSC-derived BMECs with primary pericytes and primary neural progenitor-derived astrocytes and neurons enhanced BMEC barrier tightness (*30*). Subsequently, iPSC-derived astrocytes and neurons were shown to induce barrier formation in iPSC-derived BMECs (*34*). Here, iPSC-derived brain pericyte–like cells were combined with iPSC-derived BMECs, astrocytes, and neurons to model the NVU. IMR90C4-derived BMECs were sequentially cocultured with IMR90C4-derived brain pericyte–like cells and IMR90C4-derived astrocyte/neuron cultures (PNA) and compared to IMR90C4-derived BMEC monocultures or IMR90C4-derived BMECs cocultured with pericytes (P) or astrocytes/neurons (NA) alone (Fig. 6A). All three coculture conditions (P, NA, and PNA) significantly elevated TEER above monoculture (Fig. 6B). While neuron/astrocyte coculture slightly elevated TEER above pericyte coculture (720 ± 84 Ω·cm^2 NA coculture versus 503 ± 63 Ω·cm^2 P coculture), the combination of pericyte and neuron/astrocyte coculture treatments further elevated BMEC TEER (1156 ± 94 Ω·cm^2 versus NA and P coculture) (Fig. 6B). All three coculture conditions yielded a fivefold reduction in sodium fluorescein permeability compared to monoculture conditions, but no appreciable differences were observed between separate coculture treatment conditions (Fig. 6C), as has been reported previously for BMEC monolayers, with TEER values exceeding ~500 to 600 Ω·cm^2 (*30*, *34*, *57*). These data demonstrate that iPSC-derived brain pericyte–like cells can be readily combined with iPSC-derived BMECs, astrocytes, and neurons to form an isogenic model of the human NVU.

DISCUSSION

Brain pericytes play essential roles in BBB formation and maintenance by regulating BMEC transcytosis, barrier fidelity, vascular structure, and stability (*5*, *13*, *14*, *19*–*21*). Here, we report that mural cells can be differentiated from hPSC-derived NCSCs and that these cells develop brain pericyte–like attributes. The brain pericyte–like cells can self-assemble with endothelial cells in vitro and affect their vascular network structure. Moreover, the brain pericyte–like cells induce BBB properties, including barrier tightening and reduction of transcytosis in BMECs. Last, these cells can be incorporated into an isogenic iPSC-derived NVU model, with potential applications in patient-specific NVU modeling.

During embryonic development, NCSCs are first specified at the interface between the neural plate and nonneural ectoderm and subsequently reside in the dorsal neural tube before migrating throughout the embryo and differentiating to diverse cell types (*58*). Previous NCSC differentiation protocols have relied on differentiating hPSCs to neuroectoderm and subsequently isolating NCSC subpopulations (*41*, *47*) or have used a directed WNT activation and activin/nodal inhibition approach to obtain NCSCs (*46*, *59*, *60*). We chose to use the latter approach given its simplicity and potential for highly enriched NCSC populations. BMP signaling activation was previously shown to inhibit NCSC formation (*46*); however, the need to inhibit BMP signaling during NCSC differentiation has been variable (*42*, *46*). Here, when the differentiation strategy was adapted to minimal E6 medium, inhibition of BMP signaling was necessary to efficiently direct hPSCs to p75-NGFR$^+$/HNK1$^+$ NCSCs. The NCSCs differentiated in E6-CSFD medium were a highly enriched population of multipotent cells having the capacity to form mesenchymal derivatives and peripheral neurons using multiple hPSC lines.

A common approach to differentiate mural cells from NCSCs is to supplement basal medium with PDGF-BB and TGFβ1 (*41*, *42*, *47*). Resultant cells have been shown to express calponin, SM22α, and α-SMA (*41*, *42*, *47*), but two key mural cell markers, PDGFRβ and NG2, were not previously examined. While differentiation of NCSCs in E6 medium yielded PDGFRβ$^+$ cells, neither E6 medium nor E6 medium supplemented with PDGF-BB and TGFβ1 generated cells expressing NG2. However, both calponin and SM22α were expressed even in the absence of growth factor supplementation. Instead, when E6 was supplemented with 10% FBS, the differentiating cells acquired NG2 and PDGFRβ expression and thus were classified as forebrain lineage mural cells (*40*, *49*). Recent work demonstrated pericyte differentiation from hPSC-derived cranial neural crest cells using PDGF-BB; however, 2 to 5% FBS was included in the differentiation medium (*37*). Thus, it is possible that the observed pericyte differentiation is mediated at least partially by FBS, consistent with our observations. Alternatively, the requirement of PDGF-BB may reflect differences in initial neural crest phenotypes or basal media. While others have suggested the use of serum to drive mural cell differentiation from NCSCs (*46*, *47*), these studies generated cells that were α-SMA.

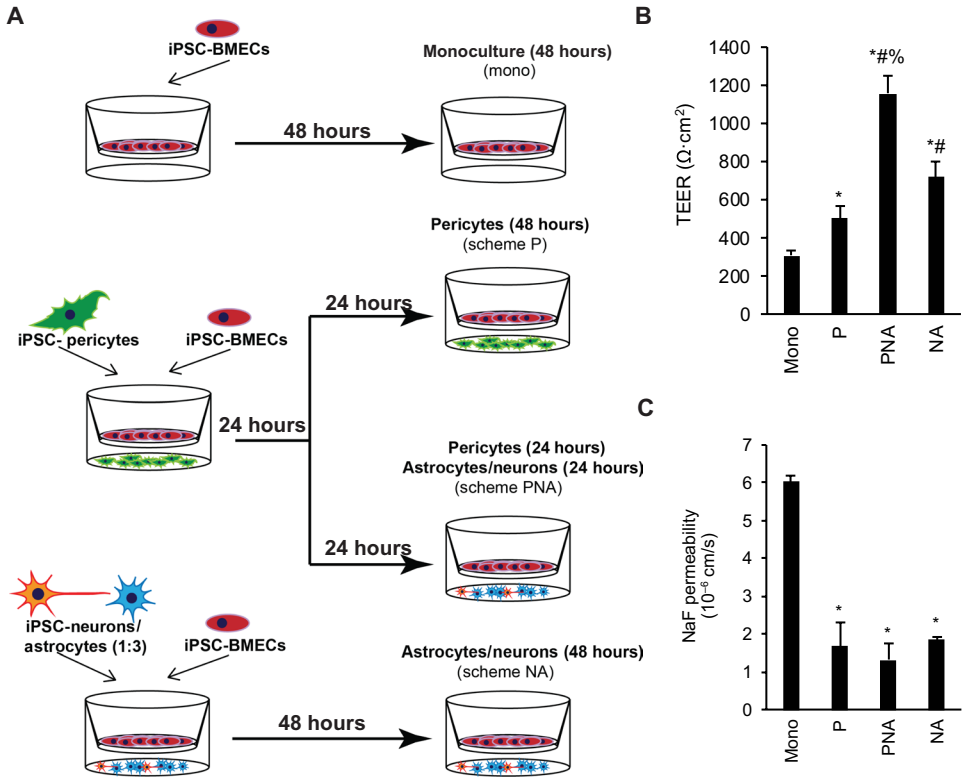

Fig. 6. IMR90C4-derived pericyte-like cells integrate into a complete isogenic NVU model. (**A**) Schematic of IMR90C4-derived BMEC coculture set up with IMR90C4-derived NVU cell types. (**B**) Maximum TEER achieved in IMR90C4-derived BMECs following monoculture or coculture. Plotted are the means ± SD from three Transwells. Results are representative of three independent differentiations. **P* < 0.05 versus monoculture, $^{\#}P$ < 0.05 versus pericyte-like cell coculture, and $^{\%}P$ < 0.05 versus astrocyte/neuron coculture, ANOVA followed by Tukey's honestly significant difference (HSD) test. (**C**) Sodium fluorescein permeability in IMR90C4-derived BMECs following 48 hours of monoculture or coculture. Plotted are the means ± SD from three Transwells. Results are representative of three independent differentiations. **P* < 0.05 versus monoculture, ANOVA followed by Tukey's HSD test.

In contrast, we did not observe substantial α-SMA expression in the differentiated mural cells, even after extended culture. Brain pericytes lining higher-order capillaries generally do not express α-SMA in vivo (*40*, *61*, *62*), although very recent evidence suggests that higher-order pericytes may actually express low levels of α-SMA that are lost upon sample preparation (*63*). In addition, it is well known that, upon fresh isolation, primary brain pericytes express α-SMA in 5 to 10% of cells, whereas after a few days in culture, they become nearly uniformly α-SMA^{+} (*38*, *39*), as also observed here with primary human brain pericytes, which expressed α-SMA. Thus, the lack of α-SMA expression in the differentiated brain pericyte–like cells better reflects the lack of α-SMA in brain pericytes in vivo. However, much like primary brain pericytes and previous reports with NCSC-derived mural cells, we observed sustained expression of the contractile-related proteins calponin and SM22α. In addition, differentiation of mesenchymoangioblasts toward pericyte lineages yielded cells that expressed differential levels of calponin (*64*). Although SM22α is an early developmental marker of mural cells (*65*), a recent single-cell transcriptomics study strongly suggests that murine brain capillary pericytes in vivo do not express calponin-encoding *Cnn1* or SM22α-encoding *Tagln* (*40*). Additional transcript evaluation confirmed the brain signature of the pericyte-like cells (*ZIC1* and *FOXF2*) (*54*, *55*). The brain pericyte–like cells also expressed transcripts for *ABCC9* and *KCNJ8*, two additional markers that differentiate brain capillary pericytes from other mural cell types (*40*, *49*), and these markers were further elevated over extended culture times. RNA-seq also indicated a transcriptome-wide similarity to primary human brain pericytes and expression of many genes identified as pericyte-enriched by single-cell RNA-seq in mouse (*40*). Together, the hPSC-derived brain pericyte–like cells had marker profiles that suggested the generation of cells similar to brain pericytes.

While the marker expression suggested that the differentiation process generated brain pericyte–like cells, it is most important that the cells recapitulate key functional attributes of brain pericytes. When cultured with HUVECs or hBMECs, brain pericyte–like cells aligned along vascular cords and extended cell processes. Primary pericytes can stabilize endothelial cell cord formation in vitro (*26*). This phenotype was also observed with both primary human brain pericytes and hPSC-derived brain pericyte–like cell coculture as indicated by reduced numbers of longer cords as has also been reported using hPSC-derived pericytes of mesenchymal origin (*64*). In addition to this more general pericyte phenotype, it was expected that a brain pericyte–like cell would affect the barrier and nonspecific transcytosis properties of brain endothelial cells (*13*, *14*). The BBB properties of both hPSC-derived BMECs and primary rat BMECs were substantially induced by coculture with hPSC-derived brain pericyte–like cells, and these effects mimicked those induced by primary human brain pericytes. TEER was increased substantially as expected (*13*, *30*). Correlating with this increased barrier function, pericyte coculture decreased the number of frayed occludin tight

junctions, as seen previously for a variety of barrier inductive stimuli (*29*, *34*, *66*), but did not alter the expression levels of tight junction proteins occludin or claudin-5. These results mirror those in vivo where tight junction structure was altered by pericytes, although the expression levels of tight junction proteins were not affected (*13*). We also demonstrated that nonspecific cellular accumulation and transcytosis were down-regulated in BMECs after coculture with brain pericyte–like cells, and the effects were indistinguishable from those elicited by primary human brain pericytes. These phenotypes combined with the developmental origins and marker expression profile, along with the similarities to primary human brain pericytes, suggest that we have generated hPSC-derived cells that can model human brain pericytes.

While many studies have used primary brain pericytes to enhance BMEC barrier properties, primary brain pericytes offer limited scalability, especially for human in vitro BBB models (*28*, *30*, *67*). In addition, limited primary cell availability essentially eliminates the possibility of using patient-matched brain pericytes and BMECs that could be used for disease modeling applications. Here, we demonstrate the capability to differentiate brain pericytes-like cells in a scalable fashion (~1000 brain pericyte–like cells per input stem cell). Moreover, the differentiation is reproducible among differentiations and across hPSC lines. Thus, the ability to derive brain pericyte–like cells from patient-derived iPSCs provides a unique tool for the study of patient-specific pericyte contributions to CNS disorders that have been suggested to have pericyte involvement, such as stroke, epilepsy, demyelinating disease, and Alzheimer's disease (*7*, *10*, *68*–*71*). In addition, lineage-specific differences have been noted in hPSC-derived pericytes, motivating the use of pericytes from appropriate developmental origins for disease modeling applications (*41*). The brain pericyte–like cells can also be used in multicellular NVU models to capture the cellular cross-talk that is likely responsible for many disease processes at the BBB. To this end, we have demonstrated that it is possible to generate BMECs, neurons, astrocytes, and brain pericyte–like cells from a single iPSC cell line and combine them to form an isogenic NVU model having optimal TEER. These findings followed similar trends to our earlier reports, where iPSC-derived BMEC properties were enhanced by coculture with brain pericytes and neural progenitor cell–derived astrocytes and neurons from primary sources. We note, however, that this Transwell-based model lacks the potentially important contributions of cell-cell contact and fluid shear stress, motivating future efforts to integrate hPSC-derived NVU cell types into microfluidic or cell aggregate–based in vitro models (*72*, *73*). It is likely that these multicellular NVU models will be used to uncover new mechanisms of BBB regulation in health and disease and assist in the therapeutic development process for CNS disorders.

MATERIALS AND METHODS

hPSC maintenance

IMR90C4 and CS03n2 iPSCs and H9 hESCs were maintained on Matrigel-coated plates in E8 medium, which is Dulbecco's modified Eagle's medium (DMEM)/F12 basal medium supplemented with L-ascorbic acid-2-phosphate magnesium (64 mg/liter), sodium selenium (14 μg/liter), FGF2 (100 μg/liter), insulin (19.4 mg/liter), $NaHCO_3$ (543 mg/liter), transferrin (10.7 mg/liter), and TGFβ1 (2 μg/liter) and prepared according to Chen *et al.* (*74*). When cells reached ~70% confluence, they were passaged using Versene to new Matrigel-coated plates. For hPSCs used in BMEC differentiations, cells were maintained in mTeSR1 on Matrigel plates and passaged as previously described (*75*).

NCSC differentiation

One day before initiating NCSC differentiation, hPSCs maintained in E8 medium were singularized using Accutase and seeded at 9.1×10^4 cells/cm^2 onto Matrigel-coated plates with E8 + 10 μM Y27632. NCSC differentiation was initiated the next day by switching the medium to E6, which is DMEM/F12 basal medium supplemented with L-ascorbic acid-2-phosphate magnesium (64 mg/liter), sodium selenium (14 μg/liter), insulin (19.4 mg/liter), $NaHCO_3$ (543 mg/liter), and transferrin (10.7 mg/liter). E6 was supplemented with heparin sodium salt from porcine mucosa (22.5 mg/liter) to stabilize FGF2, 1 μM CHIR99021, 10 μM SB431542 (Tocris), FGF2 (10 μg/liter), and 1 μM dorsomorphin, hereafter labeled E6-CSFD. Cells were expanded by replacing E6-CSFD daily and passaging cells every time cells reached 100% confluence to fresh Matrigel-coated plates. During passaging, cells were singularized using Accutase and replated at a splitting density of one 6-well to six new 6-wells in E6-CSFD medium. Cells were generally passaged without 10 μM Y27632. However, to increase IMR90C4 cell line survival during first passaging following NCSC differentiation initiation, IMR90C4 cells were replated in E6-CSFD + 10 μM Y27632. Subsequent IMR90C4 NCSC expansion passages were replated without Y27632. Cells were typically passaged 2 to 3 days following NCSC differentiation initiation and subsequently passaged every 3 to 6 days depending on cell growth kinetics.

MACS of NCSCs

At D15 of E6-CSFD treatment, cells were dissociated using Accutase and labeled with NCSC microbeads (20 μl per 10^7 cells; Miltenyi), FcR blocking reagent (20 μl per 10^7 cells), and MACS buffer [60 μl per 10^7 cells; 0.5% bovine serum albumin + 2 mM EDTA in sterile phosphate-buffered saline (PBS) without Ca^{2+}/Mg^{2+}] at 4°C for 15 min. Cells were washed in MACS buffer and resuspended in 500 μl of MACS buffer per 2×10^7 cells. Cells were sorted through two LS columns (Miltenyi Biotec) according to manufacturer instructions and resuspended in E6-CSFD + 10 μM Y27632 to appropriate density for specific NCSC lineage differentiations as described below.

NCSC lineage differentiations

For differentiation of peripheral neurons, after MACS sorting, hPSC-derived NCSCs were replated on Matrigel-coated plates and expanded for 14 days in E6-CSFD. These cells were replated on Matrigel-coated 12-well plates at 5×10^4 cells/cm^2 in E6-CSFD. The following day, the medium was switched to peripheral neuron medium composed of DMEM/F12, 1× N2 supplement, BDNF (10 ng/ml), GDNF (10 ng/ml), NT-3 (10 ng/ml), NGF-β (10 ng/ml), 200 μM ascorbic acid, and 0.5 mM cyclic adenosine monophosphate and replaced every 2 days for 2 weeks.

For differentiation of mesenchymal derivatives, after MACS sorting, hPSC-derived NCSCs were replated on noncoated polystyrene plates and expanded for 11 days in E6-CSFD. For adipogenesis, expanded hPSC-derived NCSCs were seeded at a density of 10,000 cells/cm^2 and treated with adipogenic medium composed of high-glucose DMEM, 10% FBS, 1% antibiotics, insulin (1 μg/ml), 0.5 mM IBMX, and 1 μM dexamethasone (Sigma-Aldrich). For osteogenesis, the seeding density was 5000 cells/cm^2, and the cells were treated with osteogenic medium consisting of low-glucose DMEM, 10% FBS, 1% antibiotics, ascorbic acid (50 μg/ml), 10 mM β-glycerophosphate, and 0.1 μM

dexamethasone. For chondrogenesis, 250,000 NCSCs were collected to form a high cell density pellet by centrifugation at 600*g* for 5 min and treated with chondrogenic medium containing high-glucose DMEM, 1% antibiotics and ITS Premix (BD Biosciences), L-proline (40 μg/ml), ascorbic acid (50 μg/ml), 0.9 mM sodium pyruvate (Sigma-Aldrich), 0.1 μM dexamethasone, and freshly added TGFβ1 (10 ng/ml; Peprotech). The medium was changed every 3 days for all three differentiation procedures.

To analyze adipogenic differentiation, cells were fixed in 4% formaldehyde and stained with Oil Red O (Sigma-Aldrich) for lipid droplet formation. To analyze osteogenic differentiation, cells were fixed in 60% isopropanol and stained with Alizarin red (Rowley Biochemical, Danvers, MA, USA) to evaluate mineral deposition. Chondrogenic potential was assessed by Alcian blue staining. Cell pellets were first fixed in 4% formaldehyde for 2 hours. Next, the cell pellet was dehydrated by a series of increasing concentration of ethanol, infiltrated with xylene, and then embedded with paraffin. Embedded cell pellets were cut into 8-μm sections using a microtome and stained with Alcian blue (Polysciences, Warrington, PA, USA) to determine the glycosaminoglycan content.

Pericyte differentiation factor identification

Following MACS sorting, NCSCs were replated onto 48-well plates in E6-CSFD medium + 10 μM Y27632. Cells were switched to mural cell differentiation medium the next day, expanded for 6 days, and stained for NG2/PDGFRβ expression. Cells were expanded on uncoated plates in E6 medium, E6 medium supplemented with TGFβ1 (2 ng/ml) + PDGF-BB (20 ng/ml), or E6 medium supplemented with 10% FBS. Cells were also expanded in E6 supplemented with 10% FBS on gelatin-coated plates prepared by coating plates for at least 1 hour at 37°C with a 0.1% gelatin A solution dissolved in water.

Immunocytochemistry

Cells were fixed for 15 min at room temperature with either 4% paraformaldehyde (PFA) or 100% ice-cold methanol depending on antibody staining conditions. Cells were rinsed three times in PBS without Ca^{2+}/Mg^{2+} and stored at 4°C in PBS until ready to stain. After aspirating PBS, cells were blocked for 1 hour in blocking buffer at room temperature and incubated overnight at 4°C on a rocking platform with primary antibodies diluted in primary antibody staining buffer. Antibodies and staining conditions are listed in table S1A. The following day, cells were washed three times with PBS and incubated with secondary antibodies diluted 1:200 in primary antibody staining buffer. Cells were probed for 1 hour in the dark at room temperature on a rocking platform. Afterward, secondary antibody staining buffer was aspirated, and cells were incubated for 5 min with 4 μM Hoechst 33342 diluted in PBS. Cells were washed three times with PBS and stored at 4°C in PBS in the dark until ready to image. Images were taken on Olympus epifluorescence and Nikon A1R-Si+ confocal microscopes.

Flow cytometry

Cells were incubated for 30 min on ice with primary antibody diluted in 100 μl of primary antibody staining buffer per sample as indicated in table S1A. Cells were washed one time with cold PBS (p75-NGFR/HNK1 flow cytometry) or MACS buffer (NG2 and PDGFRβ flow cytometry). Cells were subsequently incubated in 100 μl of primary antibody staining buffer with 1:500 Alexa-tagged isotype-specific goat secondary antibodies. Cells were washed as previously described and resuspended in 4% PFA for 15 min at room temperature. Cells were subsequently stored in wash buffer for up to 24 hours at 4°C before running samples on a cytometer.

Temporal RNA analysis

Cells were harvested using Accutase, quenched in DMEM/F12, and spun down for 5 min at 200*g*. After removing the supernatant, cell pellets were snap-frozen at −80°C until ready for mRNA extraction. The RNeasy Mini Kit (Qiagen) was used to extract mRNA, including a cell lysate homogenization step on QIAshredder columns (Qiagen), according to manufacturer instructions. DNA was removed on column using the RNase-free DNase Set (Qiagen). Extracted RNA was stored in nuclease-free water at −20°C until ready to reverse transcribe to complementary DNA (cDNA). RNA was reverse-transcribed at a concentration of 250 ng/ml into cDNA using an OmniScript Reverse Transcriptase Kit (Qiagen) and Oligo$(dT)_{20}$ Primers (Life Technologies). Temporal gene expression analysis was conducted using 25-μl reactions containing GoTaq Green Master Mix (Promega), 10 ng of cDNA template per reaction, and 100 nM forward/reverse primers. PCR was run according to manufacturer protocols, and all reactions included a no template and no reverse transcription control to verify the absence of genomic DNA contamination or amplification. PCR primer sequences, annealing temperatures, and cycle times are listed in table S1B. PCR products were resolved on a 2% agarose gel, stained using ethidium bromide, and imaged on a ChemiDoc XRS+ System (Bio-Rad).

RNA sequencing

RNA was extracted from H9 hESCs; H9-derived NCSCs at D15; H9-derived NCSCs maintained for 40 additional days in E6-CSFD (D55); H9-derived pericyte-like cells at D19, D22, and D25 (three independent differentiations at the D25 time point); H9-derived pericyte-like cells maintained for 20 additional days in E6 + 10% FBS (D45); CS03n2-derived pericyte-like cells at D25; IMR90C4-derived pericyte-like cells at D25; and primary brain pericytes using the RNeasy Mini Kit (Qiagen) as described above. TruSeq stranded mRNA libraries were prepared, cDNA-synthesized, pooled, and distributed over two sequencing lanes, and samples were sequenced on an Illumina HiSeq 2500 at the University of Wisconsin–Madison Biotechnology Center. Reads were mapped to the human genome (hg38) with HISAT2 (v2.1.0), and transcript abundances (FPKM) were quantified with Cufflinks (v2.1.1). FPKM values from the two sequencing lanes for each sample were averaged. Hierarchical clustering was performed with Morpheus (https://software.broadinstitute.org/morpheus) using the one minus Pearson correlation with average linkage. GO analysis was performed using the PANTHER (*76*) online tool (http://pantherdb.org).

Matrigel cord formation assay and quantification

HEK293 fibroblasts and HUVECs were maintained on tissue culture polystyrene flasks in DMEM + 10% FBS. Immortalized hBMECs (*77*), a gift of K. S. Kim and M. Stins (Johns Hopkins University, Baltimore, MD), were maintained in RPMI 1640 + 10% FBS + 10% NuSerum + 1× minimum essential medium (MEM) nonessential amino acids on flasks that had been coated with a solution of 1% rat tail collagen in 70% ethanol that was allowed to evaporate. Eight-well glass chamber slides were coated with 200 μl of concentrated growth factor reduced Matrigel per well and incubated at least 1 hour at 37°C to set the Matrigel. HUVECs or hBMECs were plated at 2.2×10^4 cells per eight-well chamber slide in 500 μl of Endothelial cell growth medium-2 (EGM-2) medium (Lonza) alone or with 6.6×10^4 HEK293 fibroblasts, primary brain pericytes, or hPSC-derived mural cells at D22 of

the differentiation. Cells were incubated for 24 hours at 37°C to allow cord formation, and bright-field images were taken on live cells at 24 hours following plating. Cords were subsequently fixed and stained according to the immunocytochemistry methods listed above. Matrigel-associated cords were mounted onto glass slips and imaged using Olympus epifluorescence and Nikon A1R-Si+ confocal microscopes. Cord length and number of cords per field were quantified by hand using the ImageJ ROI manager tool and averaged over at least three independent fields per condition per differentiation.

BMEC differentiation

IMR90C4 iPSCs were maintained in mTesR1 medium on Matrigel-coated plates and passaged as previously described. Three days before initiating a differentiation, cells were seeded at 9×10^4 to 10^5 cells/cm^2 onto Matrigel-coated plates in mTeSR1 + 10 μM Y27632. Medium was replaced daily until cells reached >2.6×10^5 cells/cm^2. Cell medium was replaced with unconditioned medium (UM), containing 392.5 ml of DMEM/F12, 100 ml of knockout serum replacement (Gibco), 5 ml of 100× MEM nonessential amino acids (Gibco), 2.5 ml of 100× GlutaMAX (Gibco), and 3.5 μl of β-mercaptoethanol. Cells were replaced daily with UM for 6 days and subsequently switched to endothelial cell (EC) medium, containing human endothelial serum-free medium + 1% platelet-poor plasma-derived serum (PDS) and FGF2 (20 ng/ml). Cells were incubated for 2 days with EC medium without replacing medium. Cells were subcultured at D8 onto 4:1:5 collagen/fibronectin/water-coated Transwells or 5× diluted 4:1:5 collagen/fibronectin/water-coated plates as detailed by Stebbins *et al.* (*75*). Cell culture medium was replaced with EC without FGF2 24 hours after subculturing hPSC-derived BMECs onto filters.

BMEC/pericyte coculture

Primary brain pericytes, hPSC-derived pericyte-like cells, and 3T3s were separately seeded onto poly-L-lysine–coated 12-well plates (primary brain pericytes) or uncoated plates (hPSC-derived early mural cells and 3T3s) when early mural cells first reached 80 to 100% confluence, typically 3 to 4 days after initiating serum treatment on hPSC-derived NCSCs (D19 to D20). Cells were plated on the same day at equivalent seeding densities of 5×10^4 cells per 12-well in either DMEM + 10% FBS (primary brain pericytes and 3T3s) or E6 + 10% FBS (hPSC-derived pericyte-like cells). Cells were dissociated with either 0.25% trypsin/EDTA (primary brain pericytes and 3T3s) or Accutase (hPSC-derived pericyte-like cells). hPSC-derived brain pericyte–like cell medium was replaced daily with E6 + 10% FBS until D22 of the differentiation. Pericytes and 3T3s were fed with DMEM + 10% FBS every 2 days until D22. At D22, cells were replaced with 1.5 ml of EC medium above 12-well polystyrene Transwell filters with a 0.4-μm pore size.

IMR90C4 iPSC-derived BMECs at D8 of the BMEC differentiation were subcultured onto Transwell filters at 1.1×10^6 cells per 12-well filter as previously described (*75*). The high seeding density is intended to ensure a confluent monolayer suitable for TEER and permeability measurements. Cells were incubated for 2 days in coculture, with cell culture medium replaced at 24 hours after initiating coculture with EC medium without FGF2. TEER was measured every 24 hours after initiating coculture. Forty-eight hours following coculture, BMEC Transwell filters were transferred to a fresh 12-well plate for sodium fluorescein assays. Cell medium was replaced with 1.5 ml of EC medium without FGF2 in the basolateral chamber and 0.5 ml of the same medium with 10 μM sodium fluorescein in the apical chamber. Cells were incubated for 1 hour on a rotating platform, and basolateral chamber medium was collected every 15 min during the 1-hour incubation period. After 1 hour, cell culture medium for the apical chamber was collected to calculate sodium fluorescein permeability across BMEC monolayers following 48 hours of coculture treatment. Fluorescence intensity was measured using a Tecan plate reader set to 485-nm excitation and 530-nm emission settings. Permeability calculations were determined according to Stebbins *et al.* (*75*).

Transcytosis and accumulation assays

Following 48 hours of coculture, BMEC-seeded Transwells were transferred to an empty plate. We used 10-kDa dextran tagged with Alexa 488 to quantify the level of intracellular accumulation and transcytosis. Dextran (10 μM) was suspended in 0.5 ml of EC medium without FGF2 onto the apical side of the Transwell. To determine the level of transcytosis, following 2 hours of incubation in a 37°C incubator (20% O_2, 5% CO_2) on a rotating platform, we collected 150 μl from the 1.5 ml of EC medium on the basolateral side of the Transwell. Fluorescence intensity was measured using a Tecan plate reader set to 495-nm excitation and 519-nm emission settings. To determine the level of accumulation (endocytosis) in the BMECs, we rinsed the Transwells with cold PBS (2×) and lysed the cells with radioimmunoprecipitation assay (RIPA) buffer. Lysates were collected and analyzed on the plate reader. Fluorescence values were normalized to protein content per Transwell measured using the bicinchoninic acid (BCA) assay.

Tight junction image analysis

BMECs were plated on 24-well plates in EC medium or EC medium conditioned by primary brain pericytes or hPSC-derived pericyte-like cells. After 48 hours, BMECs were fixed and stained for occludin as described above. Images were acquired from five wells per experimental condition. To quantify tight junction continuity, images were blinded and the area fraction index was determined using FIJI as previously described (*78*). In addition, images were blinded, and the number of frayed junctions (Fig. 4D) was manually counted.

Isogenic model of the NVU

BMECs were differentiated from iPSCs as previously described. Singularized BMECs were seeded onto collagen IV/fibronectin-coated Transwells at day 8 of the differentiation. hPSC-derived pericytes were seeded onto the bottom of the coculture plate (~50,000 cells/cm^2) in EC medium. We additionally investigated the cumulative effects of pericytes, neurons, and astrocytes. Neurons and astrocytes were differentiated from iPSCs as previously published (*34*). Initially, BMECs were placed in coculture with pericytes for 24 hours in EC medium, and then BMEC Transwells were transferred to a coculture plate with a mixture of neurons and astrocytes (1:3 ratio) for the duration of the experiment in EC medium without FGF2. We benchmarked our stem cell–derived BBB model [BMECs, pericyte-like cells (24 hours), and neurons and astrocytes (24 hours)] to a BBB coculture model absent of pericyte-like cells (neurons and astrocytes only). TEER and sodium fluorescein permeability assays were conducted on BMEC Transwells.

Statistics

All experiments were conducted using at least three technical replicates (e.g., three 6-wells or Transwells) from the same differentiation. All experiments were replicated (independent differentiations)

at least three times except where otherwise indicated. Data are presented as means ± SD of technical replicates from a representative differentiation or as means ± SEM of pooled data from several independent differentiations. Statistical significance was evaluated using one-way analysis of variance (ANOVA), followed by post hoc tests controlling for multiple comparisons, Dunnett's test for comparison of experimental groups to control, and Tukey's test for comparison between all experimental groups. $P < 0.05$ was considered statistically significant.

Western blotting

BMECs were cultured on Transwells alone or cocultured with hPSC-derived pericyte-like cells, primary brain pericytes, or 3T3s as previously described. After 48 hours of coculture, BMECs were washed once with PBS and lysed with RIPA buffer + Halt protease inhibitor cocktail. The BCA assay was used to determine protein concentration. Proteins were resolved on 4 to 12% tris-glycine gels and transferred to nitrocellulose membranes, which were blocked in tris-buffered saline + 0.1% Tween 20 (TBST) + 5% nonfat dry milk for 1 hour, and incubated with primary antibodies (table S1A) overnight at 4°C. Membranes were washed with TBST (5×) and incubated with donkey anti-mouse or donkey anti-rabbit IRDye 800CW secondary antibodies (LI-COR) for 1 hour. Membranes were washed with TBST (5×) and imaged using LI-COR Odyssey.

Visualization of dextran accumulation

iPSC-derived BMECs were seeded onto glass bottom plates at a density of 10^5 cells/cm^2 and cultured for 48 hours in EC medium or EC medium conditioned by 3T3s, primary pericytes, or IMR90C4-derived pericyte-like cells. Medium was subsequently replaced with EC medium + 10 μM Alexa 488–tagged 10-kDa dextran. Following 2 hours of dextran incubation, cells were fixed in 4% PFA for 15 min, followed by three washes in PBS. Cells were blocked in 10% goat serum in PBS for 30 min at room temperature. Cells were incubated with anti–Alexa 488 antibody (1:100 in PBS; Life Technologies 11094) overnight at 4°C on a rocking platform. Following three washes in PBS, cells were incubated with Alexa 647 secondary antibody (1:200 in PBS) for 1 hour at room temperature on a rocking platform. Nuclei were labeled with Hoechst, and cells were rinsed three times in PBS. Cells were visualized on a Nikon A1R-Si+ confocal microscope. The lack of permeabilization allows internalized dextran to be visualized only with Alexa 488, while extracellular (surface) dextran is also labeled with Alexa 647.

Primary rat BMEC/pericyte coculture

All animal studies were conducted using protocols approved by the University of Wisconsin–Madison Animal Care and Use Committee following National Institutes of Health (NIH) guidelines for care and use of laboratory animals. Adult male Sprague-Dawley rat (Harlan Inc., Indianapolis, IN) brain capillaries were isolated, minced, and digested in collagenase type 2 (0.7 mg/ml) and deoxyribonuclease I (DNase I) (39 U/ml). Purified microvessels were isolated following centrifugation in 20% BSA and further digested in collagenase/dispase (1 mg/ml) and DNase I. To purify the population, a 33% Percoll gradient was used. Capillaries were collected and plated onto collagen IV/fibronectin-coated Transwells. Capillaries were cultured in DMEM supplemented with FGF2 (1 ng/ml), heparin (1 μg/ml), 20% PDS, 2 mM L-glutamine, and 1% antibiotic-antimitotic solution. Pure populations were obtained by treating the cells with puromycin (4 μg/ml) for 2 days following seeding. Four days following isolation, rat BMEC-seeded Transwells were transferred onto plates containing IMR90C4-derived pericyte-like cells, primary brain pericytes, or 3T3s (described previously) and cocultured in EC medium containing 1% PDS.

SUPPLEMENTARY MATERIALS

Supplementary material for this article is available at http://advances.sciencemag.org/cgi/content/full/5/3/eaau7375/DC1

Fig. S1. Generation of multipotent NCSC populations from multiple hPSC lines.
Fig. S2. Serum treatment directs iPSC-derived NCSCs toward mural cells.
Fig. S3. Supplemental analysis of hPSC-derived pericyte-like cells.
Fig. S4. Supplemental analysis of BMEC/hPSC-derived pericyte-like cell cocultures.
Fig. S5. Measurement of the effects of hPSC-derived pericyte-like cells on primary rat BMEC phenotypes.
Fig. S6. NCSCs maintained in E6-CSFD retain neural crest marker expression and do not develop pericyte marker expression.
Fig. S7. hPSC-derived pericyte-like cell assembly with brain endothelial cells.
Table S1. Antibody staining conditions and DNA primer sequences and running conditions.
Table S2. Pericyte-enriched genes identified by single-cell RNA-seq in mouse (*40*) with human homologs.
Table S3. RNA-seq FPKM data for all samples.

REFERENCES AND NOTES

1. A. R. Jones, E. V. Shusta, Blood-brain barrier transport of therapeutics via receptor-mediation. *Pharm. Res.* **24**, 1759–1771 (2007).
2. J. M. Lajoie, E. V. Shusta, Targeting receptor-mediated transport for delivery of biologics across the blood-brain barrier. *Annu. Rev. Pharmacol. Toxicol.* **55**, 613–631 (2015).
3. Y. J. Yu, R. J. Watts, Developing therapeutic antibodies for neurodegenerative disease. *Neurotherapeutics* **10**, 459–472 (2013).
4. B. V. Zlokovic, Neurovascular pathways to neurodegeneration in Alzheimer's disease and other disorders. *Nat. Rev. Neurosci.* **12**, 723–738 (2011).
5. R. D. Bell, E. A. Winkler, A. P. Sagare, I. Singh, B. LaRue, R. Deane, B. V. Zlokovic, Pericytes control key neurovascular functions and neuronal phenotype in the adult brain and during brain aging. *Neuron* **68**, 409–427 (2010).
6. A. P. Sagare, R. D. Bell, B. V. Zlokovic, Neurovascular dysfunction and faulty amyloid β-peptide clearance in Alzheimer disease. *Cold Spring Harb. Perspect. Med.* **2**, a011452 (2012).
7. A. P. Sagare, D. Bell, Z. Zhao, Q. Ma, E. A. Winkler, A. Ramanathan, B. V. Zlokovic, Pericyte loss influences Alzheimer-like neurodegeneration in mice. *Nat. Commun.* **4**, 2932 (2013).
8. Z. Zhao, A. P. Sagare, Q. Ma, M. R. Halliday, P. Kong, K. Kisler, E. A. Winkler, A. Ramanathan, T. Kanekiyo, G. Bu, N. C. Owens, S. V. Rege, G. Si, A. Ahuja, D. Zhu, C. A. Miller, J. A. Schneider, M. Maeda, T. Maeda, T. Sugawara, J. K. Ichida, B. V. Zlokovic, Central role for PICALM in amyloid-β blood-brain barrier transcytosis and clearance. *Nat. Neurosci.* **18**, 978–987 (2015).
9. E. A Winkler, Y. Nishida, A. P. Sagare, S. V. Rege, R. D. Bell, D. Perlmutter, J. D. Sengillo, S. Hillman, P. Kong, A. R. Nelson, J. S. Sullivan, Z. Zhao, H. J. Meiselman, R. B. Wendy, J. Soto, E. D. Abel, J. Makshanoff, E. Zuniga, D. C. De Vivo, B. V. Zlokovic, GLUT1 reductions exacerbate Alzheimer's disease vasculo-neuronal dysfunction and degeneration. *Nat. Neurosci.* **18**, 521–530 (2015).
10. M. R. Halliday, S. V. Rege, Q. Ma, Z. Zhao, C. A. Miller, E. A. Winkler, B. V. Zlokovic, Accelerated pericyte degeneration and blood-brain barrier breakdown in apolipoprotein E4 carriers with Alzheimer's disease. *J. Cereb. Blood Flow Metab.* **36**, 1–9 (2015).
11. B. Obermeier, R. Daneman, R. M. Ransohoff, Development, maintenance and disruption of the blood-brain barrier. *Nat. Med.* **19**, 1584–1596 (2013).
12. W. A. Banks, From blood-brain barrier to blood-brain interface: New opportunities for CNS drug delivery. *Nat. Rev. Drug Discov.* **15**, 275–292 (2016).
13. R. Daneman, L. Zhou, A. A. Kebede, B. A. Barres, Pericytes are required for blood–brain barrier integrity during embryogenesis. *Nature* **468**, 562–566 (2010).
14. A. Armulik, G. Genové, M. Mäe, M. H. Nisancioglu, E. Wallgard, C. Niaudet, L. He, J. Norlin, P. Lindblom, K. Strittmatter, B. R. Johansson, C. Betsholtz, Pericytes regulate the blood-brain barrier. *Nature* **468**, 557–561 (2010).
15. N. J. Abbott, L. Rönnbäck, E. Hansson, Astrocyte-endothelial interactions at the blood-brain barrier. *Nat. Rev. Neurosci.* **7**, 41–53 (2006).
16. G. Savettieri, I. D. Liegro, C. Catania, L. Licata, G. L. Pitarresi, S. D'Agostino, G. Schiera, V. de Caro, G. Giandalia, L. I. Giannola, A. Cestelli, Neurons and ECM regulate occludin localization in brain endothelial cells. *Neuroreport* **11**, 1081–1084 (2000).
17. G. Schiera, E. Bono, M. P. Raffa, A. Gallo, G. L. Pitarresi, I. Liegro, G. Savettieri, Synergistic effects of neurons and astrocytes on the differentiation of brain capillary endothelial cells in culture. *J. Cell. Mol. Med.* **7**, 165–170 (2003).

18. G. Schiera, S. Sala, A. Gallo, M. P. Raffa, G. L. Pitarresi, G. Savettieri, I. D. Liegro, Permeability properties of a three-cell type in vitro model of blood-brain barrier. *J. Cell. Mol. Med.* **9**, 373–379 (2005).
19. C. M. Peppiatt, C. Howarth, P. Mobbs, D. Attwell, Bidirectional control of CNS capillary diameter by pericytes. *Nature* **443**, 700–704 (2006).
20. L. Díaz-Flores, R. Gutiérrez, J. F. Madrid, H. Varela, F. Valladares, E. Acosta, P. Martín-Vasallo, L. Díaz-Flores Jr., Pericytes. Morphofunction, interactions and pathology in a quiescent and activated mesenchymal cell niche. *Histol. Histopathol.* **24**, 909–969 (2009).
21. N. B. Hamilton, D. Attwell, C. N. Hall, Pericyte-mediated regulation of capillary diameter: A component of neurovascular coupling in health and disease. *Front. Neuroenerg.* **2**, 1 (2010).
22. P. Saharinen, L. Eklund, J. Miettinen, R. Wirkkala, A. Anisimov, M. Winderlich, A. Nottebaum, D. Vestweber, U. Deutsch, G. Y. Koh, B. R. Olsen, K. Alitalo, Angiopoietins assemble distinct Tie2 signalling complexes in endothelial cell-cell and cell-matrix contacts. *Nat. Cell Biol.* **10**, 527–537 (2008).
23. A. N. Stratman, K. M. Malotte, R. D. Mahan, M. J. Davis, G. E. Davis, Pericyte recruitment during vasculogenic tube assembly stimulates endothelial basement membrane matrix formation. *Blood* **114**, 5091–5101 (2009).
24. R. J. Van Geest, I. Klaassen, I. M. C. Vogels, C. J. F. Van Noorden, R. O. Schlingemann, Differential TGF-β signaling in retinal vascular cells: A role in diabetic retinopathy? *Invest. Ophthalmol. Visual Sci.* **51**, 1857–1865 (2010).
25. A. Ben-Zvi, B. Lacoste, E. Kur, B. J. Andreone, Y. Mayshar, H. Yan, C. Gu, Mfsd2a is critical for the formation and function of the blood-brain barrier. *Nature* **509**, 507–511 (2014).
26. R. J. Bodnar, M. E. Rodgers, W. C. W. Chen, A. Wells, Pericyte regulation of vascular remodeling through the CXC receptor 3. *Arterioscler. Thromb. Vasc. Biol.* **33**, 2818–2829 (2013).
27. R. Cecchelli, S. Aday, E. Sevin, C. Almeida, M. Culot, L. Dehouck, C. Coisne, B. Engelhardt, M. P. Dehouck, L. Ferreira, A stable and reproducible human blood-brain barrier model derived from hematopoietic stem cells. *PLOS ONE* **9**, e99733 (2014).
28. S. Nakagawa, M. A. Deli, S. Nakao, M. Honda, K. Hayashi, R. Nakaoke, Y. Kataoka, M. Niwa, Pericytes from brain microvessels strengthen the barrier integrity in primary cultures of rat brain endothelial cells. *Cell. Mol. Neurobiol.* **27**, 687–694 (2007).
29. S. Nakagawa, M. A. Deli, H. Kawaguchi, T. Shimizudani, T. Shimono, Á. Kittel, K. Tanaka, M. Niwa, A new blood–brain barrier model using primary rat brain endothelial cells, pericytes and astrocytes. *Neurochem. Int.* **54**, 253–263 (2009).
30. E. S. Lippmann, A. Al-Ahmad, S. M. Azarin, S. P. Palecek, E. V. Shusta, A retinoic acid-enhanced, multicellular human blood-brain barrier model derived from stem cell sources. *Sci. Rep.* **4**, 4160 (2014).
31. P. A. Clark, A. J. al-Ahmad, T. Qian, R. R. Zhang, H. K. Wilson, J. P. Weichert, S. P. Palecek, J. S. Kuo, E. V. Shusta, Analysis of cancer-targeting alkylphosphocholine analogue permeability characteristics using a human induced pluripotent stem cell blood-brain barrier model. *Mol. Pharm.* **13**, 3341–3349 (2016).
32. G. D. Vatine, A. Al-Ahmad, B. K. Barriga, S. Svendsen, A. Salim, L. Garcia, V. J. Garcia, R. Ho, N. Yucer, T. Qian, R. G. Lim, J. Wu, L. M. Thompson, W. R. Spivia, Z. Chen, J. Van Eyk, S. P. Palecek, S. Refetoff, E. V. Shusta, C. N. Svendsen, Modeling psychomotor retardation using iPSCs from MCT8-deficient patients indicates a prominent role for the blood-brain barrier. *Cell Stem Cell* **20**, 831–843.e5 (2017).
33. R. G. Lim, C. Quan, A. M. Reyes-Ortiz, S. E. Lutz, A. J. Kedaigle, T. A. Gipson, J. Wu, G. D. Vatine, J. Stocksdale, M. S. Casale, C. N. Svendsen, E. Fraenkel, D. E. Housman, D. Agalliu, L. M. Thompson, Huntington's disease iPSC-derived brain microvascular endothelial cells reveal WNT-mediated angiogenic and blood-brain barrier deficits. *Cell Rep.* **19**, 1365–1377 (2017).
34. S. G. Canfield, M. J. Stebbins, B. S. Morales, S. W. Asai, G. D. Vatine, C. N. Svendsen, S. P. Palecek, E. V. Shusta, An isogenic blood–brain barrier model comprising brain endothelial cells, astrocytes, and neurons derived from human induced pluripotent stem cells. *J. Neurochem.* **140**, 874–888 (2017).
35. A. Appelt-Menzel, A. Cubukova, K. Günther, F. Edenhofer, J. Piontek, G. Krause, T. Stüber, H. Walles, W. Neuhaus, M. Metzger, Establishment of a human blood-brain barrier co-culture model mimicking the neurovascular unit using induced pluri- and multipotent stem cells. *Stem Cell Rep.* **8**, 894–906 (2017).
36. M. Ribecco-Lutkiewicz, C. Sodja, J. Haukenfrers, A. S. Haqqani, D. Ly, P. Zachar, E. Baumann, M. Ball, J. Huang, M. Rukhlova, M. Martina, Q. Liu, D. Stanimirovic, A. Jezierski, M. Bani-Yaghoub, A novel human induced pluripotent stem cell blood-brain barrier model: Applicability to study antibody-triggered receptor-mediated transcytosis. *Sci. Rep.* **8**, 1873 (2018).
37. C. Griffin, R. Bajpai, Neural crest-derived human cranial pericytes model primary forebrain pericytes and predict disease-specific cranial vasculature defects. *SSRN* 10.2139/ssrn.3189103 (2018).
38. R. J. Boado, W. M. Pardridge, Differential expression of alpha-actin mRNA and immunoreactive protein in brain microvascular pericytes and smooth muscle cells. *J. Neurosci. Res.* **39**, 430–435 (1994).
39. P. Dore-Duffy, K. Cleary, *Methods in Molecular Biology* (Clifton, 2011), vol. 686, pp. 49–68.
40. M. Vanlandewijck, L. He, M. A. Mäe, J. Andrae, K. Ando, F. del Gaudio, K. Nahar, T. Lebouvier, B. Laviña, L. Gouveia, Y. Sun, E. Raschperger, M. Räsänen, Y. Zarb, N. Mochizuki, A. Keller, U. Lendahl, C. Betsholtz, A molecular atlas of cell types and zonation in the brain vasculature. *Nature* **554**, 475–480 (2018).
41. C. Cheung, A. S. Bernardo, M. W. B. Trotter, R. A. Pedersen, S. Sinha, Generation of human vascular smooth muscle subtypes provides insight into embryological origin-dependent disease susceptibility. *Nat. Biotechnol.* **30**, 165–173 (2012).
42. C. Cheung, Y. Y. T. Goh, J. Zhang, C. Wu, E. Guccione, Modeling cerebrovascular pathophysiology in amyloid-β metabolism using neural-crest-derived smooth muscle cells. *Cell Rep.* **9**, 391–401 (2014).
43. H. C. Etchevers, C. Vincent, N. M. Le Douarin, G. F. Couly, The cephalic neural crest provides pericytes and smooth muscle cells to all blood vessels of the face and forebrain. *Development* **128**, 1059–1068 (2001).
44. J. Korn, B. Christ, R. Kurz, H. Kurz, Neuroectodermal origin of brain pericytes and vascular smooth muscle cells. *J. Comp. Neurol.* **442**, 78–88 (2002).
45. G. Lee, H. Kim, Y. Elkabetz, G. al Shamy, G. Panagiotakos, T. Barberi, V. Tabar, L. Studer, Isolation and directed differentiation of neural crest stem cells derived from human embryonic stem cells. *Nat. Biotechnol.* **25**, 1468–1475 (2007).
46. L. Menendez, T. A. Yatskievych, P. B. Antin, S. Dalton, Wnt signaling and a Smad pathway blockade direct the differentiation of human pluripotent stem cells to multipotent neural crest cells. *Proc. Natl. Acad. Sci. U.S.A.* **108**, 19240–19245 (2011).
47. A. Wang, Z. Tang, X. Li, Y. Jiang, D. A. Tsou, S. Li, Derivation of smooth muscle cells with neural crest origin from human induced pluripotent stem cells. *Cells Tissues Organs* **195**, 5–14 (2012).
48. L. Menendez, M. J. Kulik, A. T. Page, S. S. Park, J. D. Lauderdale, M. L. Cunningham, S. Dalton, Directed differentiation of human pluripotent cells to neural crest stem cells. *Nat. Protoc.* **8**, 203–212 (2013).
49. L. He, M. Vanlandewijck, E. Raschperger, M. Andaloussi Mäe, B. Jung, T. Lebouvier, K. Ando, J. Hofmann, A. Keller, C. Betsholtz, Analysis of the brain mural cell transcriptome. *Sci. Rep.* **6**, 35108 (2016).
50. A. Armulik, A. Abramsson, C. Betsholtz, Endothelial/pericyte interactions. *Circ. Res.* **97**, 512–523 (2005).
51. A. Armulik, G. Genové, C. Betsholtz, Pericytes: Developmental, physiological, and pathological perspectives, problems, and promises. *Dev. Cell* **21**, 193–215 (2011).
52. V. V. Orlova, Y. Drabsch, C. Freund, S. Petrus-Reurer, F. E. van den Hil, S. Muenthaisong, P. T. Dijke, C. L. Mummery, Functionality of endothelial cells and pericytes from human pluripotent stem cells demonstrated in cultured vascular plexus and zebrafish xenografts. *Arterioscler. Thromb. Vasc. Biol.* **34**, 177–186 (2014).
53. N. Guimarães-Camboa, P. Cattaneo, Y. Sun, T. Moore-Morris, Y. Gu, N. D. Dalton, E. Rockenstein, E. Masliah, K. L. Peterson, W. B. Stallcup, J. Chen, S. M. Evans, Pericytes of multiple organs do not behave as mesenchymal stem cells in vivo. *Cell Stem Cell.* **20**, 345–359.e5 (2017).
54. A. Reyahi, A. M. Nik, M. Ghiami, A. Gritli-Linde, F. Pontén, B. R. Johansson, P. Carlsson, Foxf2 is required for brain pericyte differentiation and development and maintenance of the blood-brain barrier. *Dev. Cell* **34**, 19–32 (2015).
55. R. Daneman, L. Zhou, D. Agalliu, J. D. Cahoy, A. Kaushal, B. A. Barres, The mouse blood-brain barrier transcriptome: A new resource for understanding the development and function of brain endothelial cells. *PLOS ONE* **5**, e13741 (2010).
56. E. S. Lippmann, S. M. Azarin, J. E. Kay, R. A. Nessler, H. K. Wilson, A. al-Ahmad, S. P. Palecek, E. V. Shusta, Derivation of blood-brain barrier endothelial cells from human pluripotent stem cells. *Nat. Biotechnol.* **30**, 783–791 (2012).
57. J. L. Mantle, L. Min, K. H. Lee, Minimum transendothelial electrical resistance thresholds for the study of small and large molecule drug transport in a human in vitro blood-brain barrier model. *Mol. Pharm.* **13**, 4191–4198 (2016).
58. X. Huang, J. P. Saint-Jeannet, Induction of the neural crest and the opportunities of life on the edge. *Dev. Biol.* **275**, 1–11 (2004).
59. G. Lee, S. M. Chambers, M. J. Tomishima, L. Studer, Derivation of neural crest cells from human pluripotent stem cells. *Nat. Protoc.* **5**, 688–701 (2010).
60. C. Cheung, A. S. Bernardo, R. A. Pedersen, S. Sinha, Directed differentiation of embryonic origin-specific vascular smooth muscle subtypes from human pluripotent stem cells. *Nat. Protoc.* **9**, 929–938 (2014).
61. R. A. Hill, L. Tong, P. Yuan, S. Murikinati, S. Gupta, J. Grutzendler, Regional blood flow in the normal and ischemic brain is controlled by arteriolar smooth muscle cell contractility and not by capillary pericytes. *Neuron* **87**, 95–110 (2015).
62. H. S. Wei, H. Kang, I.-Y. D. Rasheed, S. Zhou, N. Lou, A. Gershteyn, E. D. McConnell, Y. Wang, K. E. Richardson, A. F. Palmer, C. Xu, J. Wan, M. Nedergaard, Erythrocytes are oxygen-sensing regulators of the cerebral microcirculation. *Neuron* **91**, 851–862 (2016).
63. L. Alarcon-Martinez, S. Yilmaz-Ozcan, M. Yemisci, J. Schallek, K. Kılıç, A. Can, A. di Polo, T. Dalkara, Capillary pericytes express α-smooth muscle actin, which requires prevention of filamentous-actin depolymerization for detection. *eLife* **7**, e34861 (2018).
64. A. Kumar, S. S. D'Souza, O. V. Moskvin, H. Toh, B. Wang, J. Zhang, S. Swanson, L. W. Guo, J. A. Thomson, I. I. Slukvin, Specification and diversification of pericytes and smooth muscle cells from mesenchymoangioblasts. *Cell Rep.* **19**, 1902–1916 (2017).

65. J. C. L. Zhang, S. Kim, B. P. Helmke, W. W. Yu, K. L. du, M. M. Lu, M. Strobeck, Q.-C. Yu, M. S. Parmacek, Analysis of SM22-deficient mice reveals unanticipated insights into smooth muscle cell differentiation and function. *Mol. Cell. Biol.* **21**, 1336–1344 (2001).
66. A. R. Calabria, C. Weidenfeller, A. R. Jones, H. E. De Vries, E. V. Shusta, Puromycin-purified rat brain microvascular endothelial cell cultures exhibit improved barrier properties in response to glucocorticoid induction. *J. Neurochem.* **97**, 922–933 (2006).
67. S. Dohgu, F. Takata, A. Yamauchi, S. Nakagawa, T. Egawa, M. Naito, T. Tsuruo, Y. Sawada, M. Niwa, Y. Kataoka, Brain pericytes contribute to the induction and up-regulation of blood-brain barrier functions through transforming growth factor-β production. *Brain Res.* **1038**, 208–215 (2005).
68. R. Muramatsu, M. Kuroda, K. Matoba, H. Lin, C. Takahashi, Y. Koyama, T. Yamashita, Prostacyclin prevents pericyte loss and demyelination induced by lysophosphatidylcholine in the central nervous system. *J. Biol. Chem.* **290**, 11515–11525 (2015).
69. R. Garbelli, F. de Bock, V. Medici, M. C. Rousset, F. Villani, B. Boussadia, M. Arango-Lievano, F. Jeanneteau, R. Daneman, F. Bartolomei, N. Marchi, PDGFRβ$^+$cells in human and experimental neuro-vascular dysplasia and seizures. *Neuroscience* **306**, 18–27 (2015).
70. S. Milesi, B. Boussadia, C. Plaud, M. Catteau, M.-C. Rousset, F. de Bock, M. Schaeffer, M. Lerner-Natoli, V. Rigau, N. Marchi, Redistribution of PDGFRβ cells and NG2DsRed pericytes at the cerebrovasculature after status epilepticus. *Neurobiol. Dis.* **71**, 151–158 (2014).
71. E. Gonul, B. Duz, S. Kahraman, H. Kayali, A. Kubar, E. Timurkaynak, Early pericyte response to brain hypoxia in cats: An ultrastructural study. *Microvasc. Res.* **64**, 116–119 (2002).
72. Y. I. Wang, H. E. Abaci, M. L. Shuler, Microfluidic blood–brain barrier model provides in vivo-like barrier properties for drug permeability screening. *Biotechnol. Bioeng.* **114**, 184–194 (2017).
73. T. Park, N. Mustafaoglu, A. Herland, R. M. Hasselkus, R. Mannix, E. A. FitzGerald, R. Prantil-Baun, A. Watters, O. Henry, M. Benz, H. Sanchez, H. J. McCrea, L. C. Goumnerova, H. W. Song, S. P. Palecek, E. Shusta, D. E. Ingber, Hypoxia-enhanced Blood-Brain Barrier Chip recapitulates human barrier function, drug penetration, and antibody shuttling properties. bioRxiv, 482463 (2018).
74. G. Chen, D. R. Gulbranson, Z. Hou, J. M. Bolin, V. Ruotti, M. D. Probasco, K. Smuga-Otto, S. E. Howden, N. R. Diol, N. E. Propson, R. Wagner, G. O. Lee, J. Antosiewicz-Bourget, J. M. C. Teng, J. A. Thomson, Chemically defined conditions for human iPSC derivation and culture. *Nat. Methods* **8**, 424–429 (2011).
75. M. J. Stebbins, H. K. Wilson, S. G. Canfield, T. Qian, S. P. Palecek, E. V. Shusta, Differentiation and characterization of human pluripotent stem cell-derived brain microvascular endothelial cells. *Methods* **101**, 93–102 (2016).
76. H. Mi, X. Huang, A. Muruganujan, H. Tang, C. Mills, D. Kang, P. D. Thomas, PANTHER version 11: Expanded annotation data from Gene Ontology and Reactome pathways, and data analysis tool enhancements. *Nucleic Acids Res.* **45**, D183–D189 (2017).
77. M. F. Stins, J. Badger, K. Sik Kim, Bacterial invasion and transcytosis in transfected human brain microvascular endothelial cells. *Microb. Pathog.* **30**, 19–28 (2001).
78. M. J. Stebbins, E. S. Lippmann, M. G. Faubion, R. Daneman, S. P. Palecek, E. V. Shusta, Activation of RARα, RARγ, or RXRα increases barrier tightness in human induced pluripotent stem cell-derived brain endothelial cells. *Biotechnol. J.* **13**, 1700093 (2018).

Acknowledgments: We acknowledge the University of Wisconsin–Madison Biotechnology Center Gene Expression Center and DNA Sequencing Facility for providing library preparation and next-generation sequencing services and the University of Wisconsin–Madison Biochemistry Optical Core for use of a confocal microscope. **Funding:** This work was supported by NIH grants NS083688 and NS103844 (to E.V.S., S.P.P., and R.D.) and DTRA grant HDTRA-15-1-0012 (to E.V.S.). M.J.S. and B.D.G. were supported by National Institutes of Health Biotechnology Training Program grant T32 GM008349. B.D.G. was supported by the National Science Foundation Graduate Research Fellowship Program under grant no. 1747503. **Author contributions:** M.J.S., S.P.P., and E.V.S. conceived the project. M.J.S., B.D.G., S.G.C., M.-S.L., W.-J.L., R.D., S.P.P., and E.V.S. designed and analyzed experiments. M.J.S., B.D.G., S.G.C., M.-S.L., D.R., and M.G.F. performed experiments. M.J.S., B.D.G., S.P.P., and E.V.S. wrote the manuscript. **Competing interests:** M.J.S., S.P.P., and E.V.S. are inventors on a provisional patent application related to this work filed by WARF (P170340US01, filed August 2018). The authors declare no other competing interests. **Data and materials availability:** RNA-seq data were submitted to the Gene Expression Omnibus with accession no. GSE124579. All data needed to evaluate the conclusions in the paper are present in the paper and/or the Supplementary Materials. Additional data related to this paper may be requested from the authors.

Submitted 11 July 2018
Accepted 29 January 2019
Published 13 March 2019
10.1126/sciadv.aau7375

Citation: M. J. Stebbins, B. D. Gastfriend, S. G. Canfield, M.-S. Lee, D. Richards, M. G. Faubion, W.-J. Li, R. Daneman, S. P. Palecek, E. V. Shusta, Human pluripotent stem cell–derived brain pericyte–like cells induce blood-brain barrier properties. *Sci. Adv.* **5**, eaau7375 (2019).